Resource

TRANSPARENT PROCESS OPEN ACCESS

THE EMBO JOURNAL

Spatial and proteomic profiling reveals centrosome-independent features of centriolar satellites

Ladan Gheiratmand[1], Etienne Coyaud[2], Gagan D Gupta[1,†], Estelle MN Laurent[2], Monica Hasegan[1], Suzanna L Prosser[1], João Gonçalves[1], Brian Raught[2,3,*] & Laurence Pelletier[1,4,**]

Abstract

Centriolar satellites are small electron-dense granules that cluster in the vicinity of centrosomes. Satellites have been implicated in multiple critical cellular functions including centriole duplication, centrosome maturation, and ciliogenesis, but their precise composition and assembly properties have remained poorly explored. Here, we perform *in vivo* proximity-dependent biotin identification (BioID) on 22 human satellite proteins, to identify 2,113 high-confidence interactions among 660 unique polypeptides. Mining this network, we validate six additional satellite components. Analysis of the satellite interactome, combined with subdiffraction imaging, reveals the existence of multiple unique microscopically resolvable satellite populations that display distinct protein interaction profiles. We further show that loss of satellites in PCM1-depleted cells results in a dramatic change in the satellite interaction landscape. Finally, we demonstrate that satellite composition is largely unaffected by centriole depletion or disruption of microtubules, indicating that satellite assembly is centrosome-independent. Together, our work offers the first systematic spatial and proteomic profiling of human centriolar satellites and paves the way for future studies aimed at better understanding the biogenesis and function(s) of these enigmatic structures.

Keywords BioID; centrinone; centriolar satellites; centrosome; proteomics
Subject Categories Cell Adhesion, Polarity & Cytoskeleton; Methods & Resources; Post-translational Modifications, Proteolysis & Proteomics
DOI 10.15252/embj.2018101109 | Received 10 November 2018 | Revised 9 May 2019 | Accepted 10 May 2019 | Published online 3 June 2019
The EMBO Journal (2019) 38: e101109

See also: **V Quarantotti *et al*** (July 2019)

Introduction

Centriolar satellites (also referred to here as satellite(s)) are small electron-dense granules with a diameter of ~70–100 nm that cluster in the vicinity of centrosomes (Kubo *et al*, 1999; Barenz *et al*, 2011). PCM1 was the first satellite protein identified and is thought to act as the master satellite assembly scaffold (Balczon *et al*, 1994) since it interacts with and is required for the localization of a number of other satellite components, including CCDC66 (Conkar *et al*, 2017), PIBF1 (Kim *et al*, 2012), CEP290 (Kim *et al*, 2008), CEP131 (Staples *et al*, 2012), BBS4 (Nachury *et al*, 2007), CEP72 (Stowe *et al*, 2012), and CCDC13 (Staples *et al*, 2014). Conversely, PCM1 distribution can be perturbed by manipulating other satellite proteins. For example, both the depletion and the overexpression of CEP290 result in PCM1 redistribution (Kim *et al*, 2008) and knockdown of SSX2IP or PIBF1 leads to the dispersion of PCM1 throughout the cytoplasm (Kim *et al*, 2012; Klinger *et al*, 2014). The complexity of satellite assembly/maintenance requirements was recently demonstrated in a large-scale RNAi screen of ~500 genes coding for network components of the centrosome–cilium proximity interaction landscape (Gupta *et al*, 2015). Gupta *et al* showed that knockdown of 199 of the corresponding gene products had measurable and differential effects on the intensity and distribution of PCM1- and CEP290-labeled structures in the cell. Together, these data suggest that multiple factors can affect satellite assembly, maintenance, and steady-state distribution.

Satellites are required for the correct assembly and duplication of centrosomes. For example, in the absence of PCM1, the level of certain centrosome components, including NIN, CETN2, and PCNT is markedly reduced (Dammermann & Merdes, 2002). SSX2IP/hMsd1 interacts with γ-tubulin and plays a role in microtubule anchoring and spindle assembly, and its depletion affects centrosome integrity, PCM1 recruitment, and centrosome maturation (Barenz *et al*, 2013; Hori *et al*, 2014). KIAA0753 and CCDC14, two other satellite proteins, also play a role in regulating centriole duplication (Firat-Karalar *et al*, 2014; Kodani *et al*, 2015). However, while satellites are clearly

1 Lunenfeld-Tanenbaum Research Institute, Mount Sinai Hospital, Toronto, ON, Canada
2 Princess Margaret Cancer Centre, University Health Network, Toronto, ON, Canada
3 Department of Medical Biophysics, University of Toronto, Toronto, ON, Canada
4 Department of Molecular Genetics, University of Toronto, Toronto, ON, Canada
*Corresponding author. Tel: +1416 581 7478; E-mail: brian.raught@uhnresearch.ca
**Corresponding author. Tel: +1416 586 4800 (ext. 6196); E-mail: pelletier@lunenfeld.ca
†Current address: Department of Chemistry and Biology, Ryerson University, Toronto, ON, Canada

required for centrosome integrity, the role of centrosomes in satellite assembly and function is not yet known.

In addition to the well-characterized role of satellites in centrosome biogenesis through the delivery of necessary components to centrosomes (Barenz *et al*, 2013; Firat-Karalar *et al*, 2014; Kodani *et al*, 2015), satellites are involved in a myriad of other cellular functions. Indeed, a number of studies have implicated satellites in ciliation (Lopes *et al*, 2011; Stowe *et al*, 2012; Lee & Stearns, 2013; Hori *et al*, 2014; Gupta *et al*, 2015; Conkar *et al*, 2017; Kim *et al*, 2008, 2012), autophagy (Tang *et al*, 2013; Zhang *et al*, 2016; Joachim *et al*, 2017), actin assembly and organization (Farina *et al*, 2016; Obino *et al*, 2016), cellular stress response (Villumsen *et al*, 2013), DNA damage repair (Staples *et al*, 2012, 2014), and neurogenesis (Zhang *et al*, 2016). The variety of satellite-associated functions, together with the growing number of satellite components, raises the possibility that different groups of satellites might be associated with diverse physiological roles (Hori & Toda, 2017).

Satellites are dynamic structures that move along microtubules (MT) in a dynein-dependent manner (Balczon *et al*, 1999; Dammermann & Merdes, 2002). Several studies have shown that disrupting the MT network affects satellite distribution, leading to their dispersion throughout the cytoplasm (Kim *et al*, 2008; Kodani *et al*, 2010; Lopes *et al*, 2011; Lee & Stearns, 2013; Staples *et al*, 2014; Lee *et al*, 2016; Silva *et al*, 2016; Conkar *et al*, 2017). The MT network is thus clearly important for satellite localization, but its role in satellite assembly and maintenance is not well studied.

We still know relatively little about the composition and function (s) of satellites, highlighting the need to systematically map the protein interaction landscape of satellite-resident proteins. Proximity-dependent biotin identification (BioID) has emerged as a powerful tool to study centrosomes and ciliary proteins (Roux, *et al*, 2012; Gupta *et al*, 2015). Briefly, in BioID, a mutant *E. coli* biotin ligase (BirA R118G, or BirA*) is fused in-frame to a protein of interest, and the fusion protein is expressed in a relevant biological setting. While the mutant BirA* protein can activate free biotin to the biotinoyl-AMP intermediate, it is unable to catalyze the transfer of activated biotin to a substrate protein. The abortive enzyme thus simply releases a "cloud" of reactive biotin in the vicinity of the bait protein that can react with amine groups in lysine residues in nearby polypeptides. Biotinylated proteins can be thoroughly solubilized using stringent lysis procedures, isolated using biotin–streptavidin affinity purification, and identified by mass spectrometry. BioID is thus an efficient method for characterizing protein–protein interactions (including transient ones) and is especially useful for exploring protein–protein interactions in poorly soluble structures such as centrosomes and satellites.

BioID has already been successfully applied to a number of studies involving centrosomal and centriolar satellite proteins (Comartin *et al*, 2013; Firat-Karalar *et al*, 2014; Firat-Karalar & Stearns, 2015; Gupta *et al*, 2015; Conkar *et al*, 2017). Firat-Karalar *et al* conducted BioID on five centriolar duplication and maturation factors and revealed new interactors and centriole duplication regulators, including the satellite proteins KIAA0753 and CCDC14 (Firat-Karalar *et al*, 2014; Kodani *et al*, 2015). In our previous study, BioID was performed on 58 components of the centrosome–cilium interface, including five known satellite proteins, to generate a proximity interaction landscape encompassing 1,700 unique proteins in cycling and ciliated cells where nine novel satellite proteins were identified (Gupta *et al*, 2015). However, to date, a more systematic survey of the satellite interaction landscape has been lacking.

Here, we report the spatial and proteomic profiling of 22 human satellite proteins using BioID and a low- to super-resolution automated imaging pipeline. Probing this proteome, we identify and validate six additional satellite components. Using prey-centered correlation analyses of the interactome, we also identify proteomically discernable clusters of satellites, suggestive of both unique and shared functions. We further show that satellite composition and assembly remain mostly unchanged in the absence of centrosomes and an intact MT network. However, in PCM1-depleted cells there is a dramatic change in the satellite interaction landscape. This vast and yet largely unexplored satellite protein interaction space represents a rich resource to be mined in order to further dissect the inner workings of satellites not only as it pertains to the biogenesis of these poorly understood organelles, but also in regard to their function in centrosome and cilia-related processes and myriad other cellular functions.

Results

A proximity interaction landscape of human centriolar satellites

To define the proximity interaction landscape of human satellites, we performed BioID on 22 of the 44 known satellite proteins that localize primarily to satellites (Fig 1A and Table EV1). We had previously profiled five satellite baits: OFD1, CEP290, CEP63, KIAA0753, and PCM1 (Gupta *et al*, 2015). For consistency, these baits were also included in the more comprehensive satellite analysis conducted here (see Materials and Methods). A comparison of our previously published dataset with the new BioID interactomes (analyzed on newer instruments) for these five bait proteins demonstrated a high degree of reproducibility (Appendix Fig S1).

The 22 satellite baits were fused to a FLAG-BirA* epitope tag at either their N or C terminus and stably integrated in Flp-In T-REx 293 cells as described previously (Comartin *et al*, 2013; Gupta *et al*, 2015; Yeh *et al*, 2015). The expression of the bait proteins was induced with tetracycline (Tet), and biotinylation of proximal proteins effected via the addition of exogenous biotin (Figs 1B and EV1A). For each bait protein, satellite localization was confirmed by colocalization with PCM1, and streptavidin labeling was conducted to confirm *in vivo* biotinylation at satellites (Figs 1B and EV1A). We confirmed that inducing the expression of the tagged bait proteins for 24h does not affect satellite distribution, based on PCM1 intensity and the total area occupied by satellites. This is shown in three different bait proteins (FLAG-BirA*-CEP290, FLAG-BirA*-CCDC14, and FLAG-BirA*-CEP72) with or without Tet induction (Appendix Fig S2A and B). Biotinylated proteins were recovered and identified using tandem mass spectrometry (MS-MS). Two biological replicates (each analyzed using two technical replicates) were performed for each bait protein. Significance analysis of interactome (SAINT) analysis (with Bayesian false discovery rate (BFDR) < 1%; Teo *et al* 2014) was conducted to identify high-confidence interactions using a set of 20 negative control runs, in which BioID was performed on cells expressing the FLAG-BirA* tag alone.

This analysis identified 2113 proximity interactions (PxIs) with 660 unique human proteins (Table EV2; all raw mass spectrometry

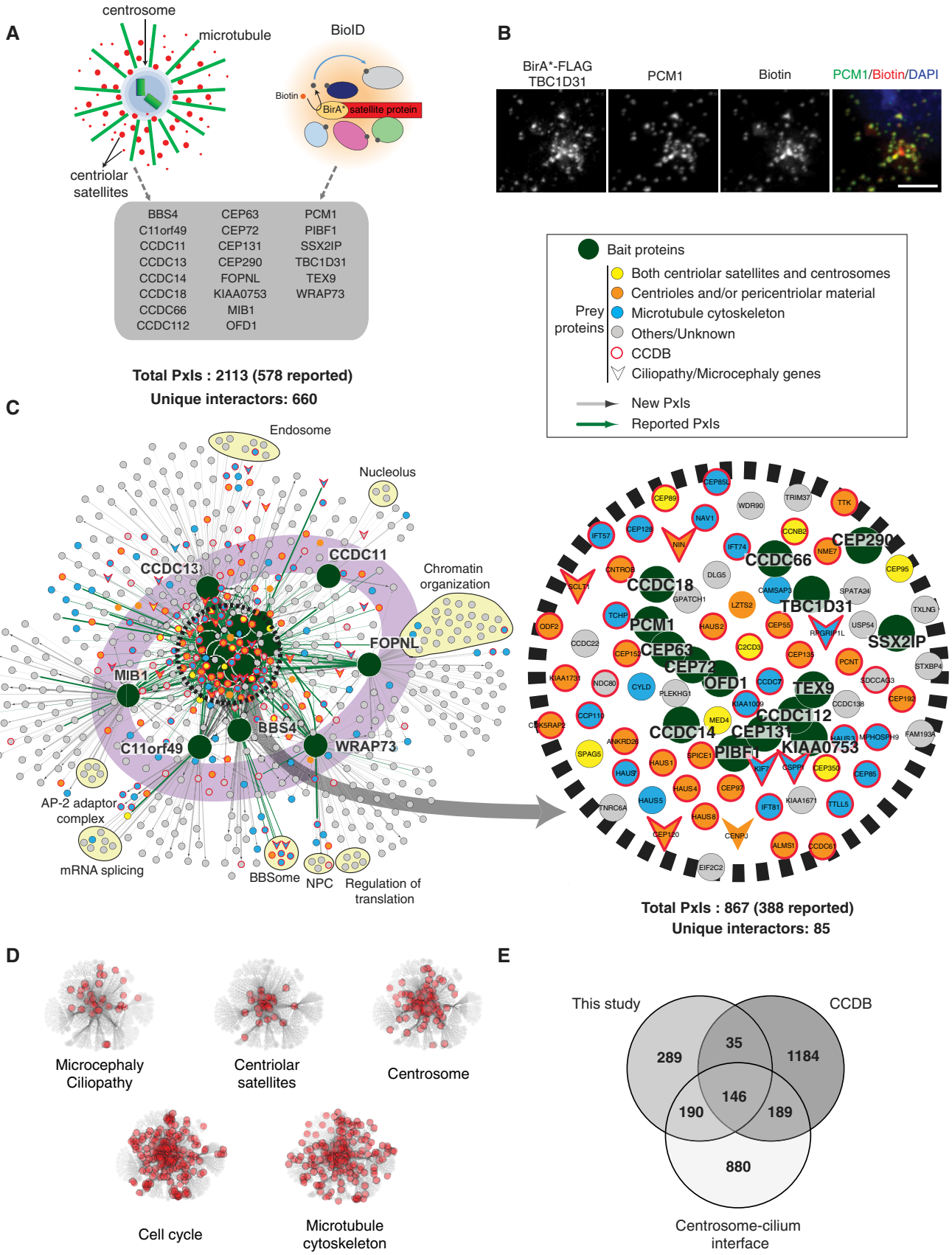
A
centrosome
microtubule
centriolar satellites
BioID
Biotin
BirA*
satellite protein
BBS4 CEP63 PCM1
C11orf49 CEP72 PIBF1
CCDC11 CEP131 SSX2IP
CCDC13 CEP290 TBC1D31
CCDC14 FOPNL TEX9
CCDC18 KIAA0753 WRAP73
CCDC66 MIB1
CCDC112 OFD1
B
BirA*-FLAG TBC1D31
PCM1
Biotin
PCM1/Biotin/DAPI
Bait proteins
Prey proteins
Both centriolar satellites and centrosomes
Centrioles and/or pericentriolar material
Microtubule cytoskeleton
Others/Unknown
CCDB
Ciliopathy/Microcephaly genes
New PxIs
Reported PxIs
Total PxIs : 2113 (578 reported)
Unique interactors: 660
C
Endosome
Nucleolus
CCDC11
CCDC13
Chromatin organization
FOPNL
MIB1
BBS4
C11orf49
WRAP73
AP-2 adaptor complex
mRNA splicing
BBSome
NPC
Regulation of translation
CCDC66
CEP290
CCDC18
TBC1D31
PCM1
SSX2IP
CEP63
CEP72
OFD1
TEX9
CCDC112
CEP131
CCDC14
KIAA0753
PIBF1
Total PxIs : 867 (388 reported)
Unique interactors: 85
D
Microcephaly Ciliopathy
Centriolar satellites
Centrosome
Cell cycle
Microtubule cytoskeleton
E
This study
CCDB
289
35
1184
146
190
189
880
Centrosome-cilium interface

Figure 1.

Figure 1. Proximity protein interaction mapping of human centriolar satellites.

A Schematic highlighting the bait proteins subjected to BioID in this analysis (see Table EV1 for more details).

B Flp-In T-REx 293 cells stably expressing Tet-inducible BirA*-FLAG-tagged TBC1D31 were fixed 24 h after incubation with Tet and biotin. Cells were stained with antibodies against FLAG, PCM1 (green), and Alexa Fluor 594-coupled streptavidin for biotinylated proteins (red), and DAPI for nucleus. Scale bar, 3 μm (see Fig EV1A for other baits).

C Self-organized network of the satellite bait–prey interactome. Highlighted is a network "core" region (dashed circle, zoomed image of the core protein population on the right) which includes prey proteins interacting with > 11 (i.e., > 50%) satellite bait polypeptides, and a peripheral ring (purple ring) encompassing the bait proteins that associate with preys in additional cellular compartments (GO terms associated with some peripheral prey groups are indicated; see Table EV3 for details). PxI, proximity interaction. Prey proteins are color-coded as indicated. Please note that except for PCM1, which is known to exclusively localize to the centriolar satellites, the rest of the proteins labeled in yellow are known to localize to both satellites and centrioles. Preys marked in orange are known to localize to centrosomes (centrioles and/or pericentriolar material) and not to centriolar satellites, as of the date of this study.

D Enriched GO categories or gene groups overlaid on thumbnails of the network topology map (see Table EV3 for details).

E Venn diagram comparing the number of high-confidence hits found in this study vs. previous publications.

data available at the MassIVE data repository, massive.ucsd.edu, accession MSV000083121). Using data-driven bait–prey interaction analysis, a topology map was built depicting the interactome of the 22 satellite bait proteins (Fig 1C and Appendix Fig S3). The satellite network displays a dense "core" of interactors. 15 of the 22 satellite baits localize to the core (here defined as those detected with 11 (50%) or more of the bait proteins; Fig 1C, dashed line, zoomed-in circle, and Fig EV2). The seven "peripheral" satellite bait proteins are connected to the core via interactions with other satellite proteins, but also associate with preys linked to other cellular structures/compartments (Fig 1C, highlighted in yellow). For example, in addition to satellite interactors, MIB1 uniquely interacts with members of the AP-2 adaptor complex (Fig 1C, e.g., AP2A1, AP2A2, AP2M1), while WRAP73 interacts with proteins linked to mRNA translation (e.g., DNAJC7, CELF1, and PUM1 and PUM2) and nuclear pore complex (NPC) proteins (Fig 1C), and BBS4 displays a unique set of interactions with the other BBSome components, a complex required for ciliogenesis (Nachury *et al*, 2007) (Fig 1C and Table EV3).

The satellite network is significantly enriched in previously identified satellite (Gene Ontology (GO):0034451), centrosomal (GO:0005813), and microtubule cytoskeleton components (GO: 0015630; GO and pathway enrichment analysis; $P < 0.001$; Fig 1C and D and Table EV3). Disease genes related to microcephaly and ciliopathy are also found in our network (Fig 1C and D), further confirming the connection between these diseases and satellite components. Despite a number of shared GO categories (Fig 1C, yellow regions and Table EV3), such as centrosome, centriolar satellites, and microtubule cytoskeleton (Table EV3), there are several groups specific to given bait proteins, suggestive of minor secondary bait localizations and/or a transient association of preys with satellite baits (*e.g.,* at a specific cell cycle stage).

We next compared the satellite interactome with our previously published centrosome–cilium interface proximity interaction dataset (Gupta *et al*, 2015). Of 660 unique interactors identified in the current study, 336 (~51%) were also reported as preys in the centrosome–cilium proteome (Gupta *et al*, 2015). Approximately 27% (181/660 preys) of this dataset overlaps with CCDB, a previously compiled centrosome and cilia database (comprising 1,554 proteins) assembled and presented by Gupta *et al* using previously published cilia and centrosome-related datasets (Table EV4) (van Dam *et al*, 2013; Alves-Cruzeiro *et al*, 2014; Gupta *et al*, 2015), confirming that our dataset is enriched in centrosome-associated proteins (Figs 1E and EV1C). Our dataset also contains 73 of 131 proteins (~56%) identified in two previous studies using the BioID approach (Firat-Karalar *et al*, 2014; Conkar *et al*, 2017), and 79 of 178 (~40%) of those detected in previous centrosome proteomics studies (Andersen *et al*, 2003; Jakobsen *et al*, 2011; Fig EV1B and Table EV4). Notably, 40% (262) of the proximal interactors identified in this study have not previously been associated with satellites (Fig EV1C). Hence, our analysis adds to the knowledge of centriolar satellite molecular interactions and provides a significant fraction of previously unexplored interaction space.

Centriolar satellites associate with proteins implicated in varied cellular functions

A heat map based on the number of baits interacting with each prey (*i.e.,* the indegree) was generated to highlight the "centrality" of each protein (Fig 2A). As expected, the majority of the prey proteins captured by more than 11 satellite baits fall into the core of the interactome (Figs 2A and EV2), and most of these interactors (~70%) were previously reported as satellite components or centrosome-related proteins. 22 satellite proteins, including 16 of our baits and all eight subunits of the HAUS (Augmin) complex, are among this group of preys (Fig EV2). The HAUS complex is evolutionarily conserved and plays a role in MT-dependent MT amplification within the mitotic spindle, and its depletion leads to spindle and centrosome integrity defects (Goshima *et al*, 2008; Lawo *et al*, 2009).

Consistent with previous reports providing evidence for links between RNA, P-bodies, and centrosomes (Aizer *et al*, 2008; Moser *et al*, 2011; Youn *et al*, 2018), components of the GW182/P-body were identified with multiple baits (Fig EV2). Multiple MT-binding and/or regulatory proteins were also detected, including CAMSAP3, a minus-end-binding protein that regulates MT dynamics and organization (Tanaka *et al*, 2012), and TTLL5, a tubulin polyglutamylase localizing to centrioles at the base of the connecting cilium in retina. Mutations in the *TTLL5* gene result in retinal dystrophy and male infertility (Lee *et al*, 2013; Sergouniotis *et al*, 2014). IFT81 and IFT74 are components of the intraflagellar transport (IFT) machinery that form a module important for the intraflagellar transport of tubulin (Lucker *et al*, 2005; Bhogaraju *et al*, 2013; Kubo *et al*, 2016). We also detected proteins involved in Hippo signaling (DLG5), cytoskeleton remodeling (TCHP), cytokine signaling (TXLNA/G) (Hotokezaka *et al*, 2015; Kwan *et al*, 2016; Liu *et al*, 2017), and intracellular trafficking (SDCCAG3; McGough *et al*, 2014), as well as a number of polypeptides with unknown function or localization (GPATCH1, CCDC138, CCDC22, CCDC77, and KIAA1671).

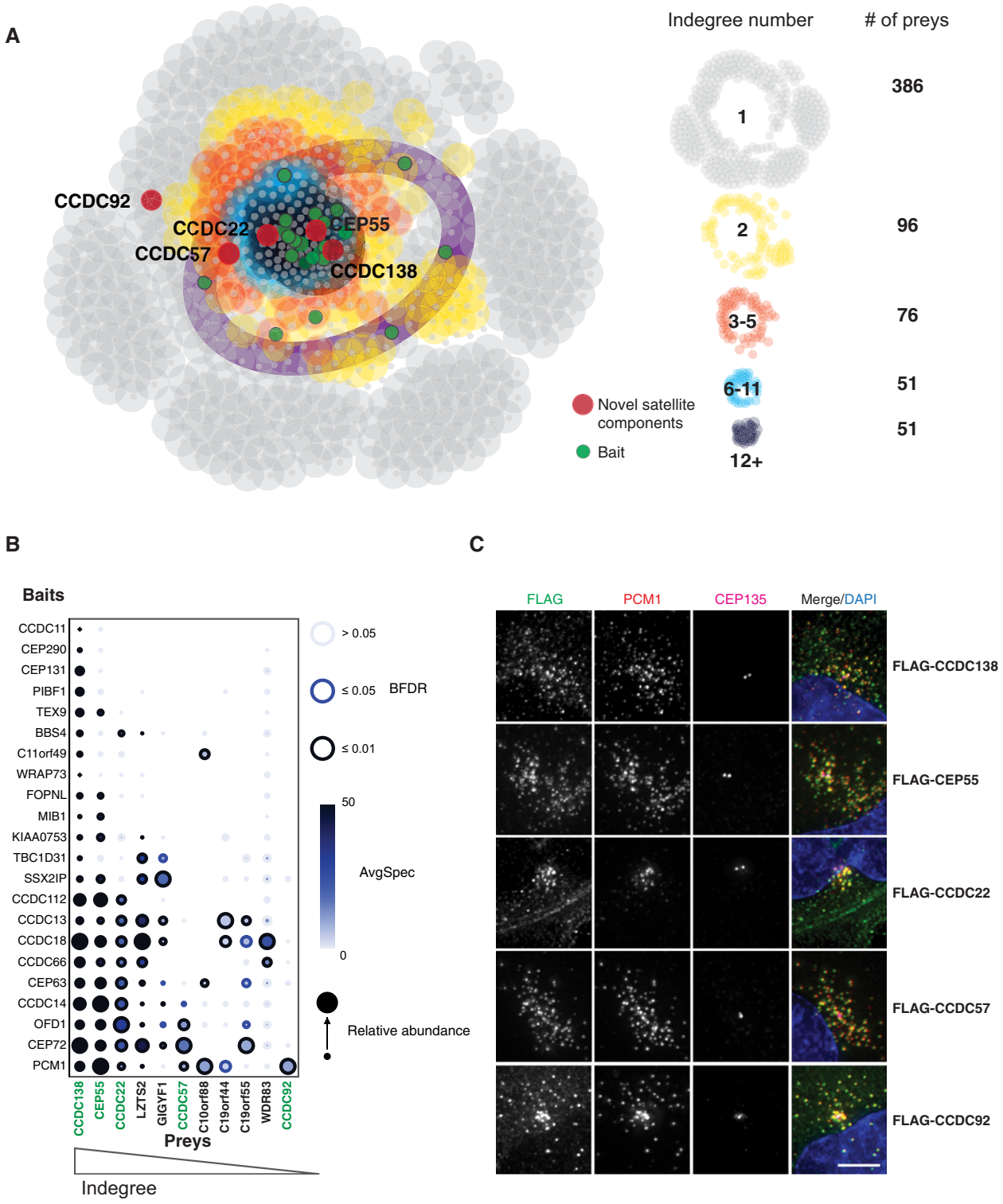

Figure 2. Identification of novel satellite components.

A Molecular heat map of the satellite network based on the number of baits that interact with each prey (i.e., indegree number). Number of preys in each color grouping shown at right. Red circles represent the satellites identified in this study.

B Interactome "dot plot" for the 11 prey proteins characterized in (C). Protein interactomes are ordered based on indegree values (x-axis). Green protein names highlight those that localize to satellites.

C hTERT RPE-1 cells transiently expressing the indicated FLAG-tagged proteins were fixed and stained with indicated antibodies. PCM1 and CEP135 were used for satellite and centriole markers, respectively. Scale bar, 5 μm.

Localization survey of core satellite network components identifies additional satellite-resident proteins

To identify novel centriolar satellite proteins, we tested 11 candidates (Fig 2B), four from the core region of the topology map (detected by 11 or more bait proteins, also bold blue fonts in Fig EV2) and seven from the peripheral region (detected by 1–5 bait proteins, Fig 2B). Interactors were selected based on the availability of full-length cDNAs coding for proteins that are either uncharacterized (C19orf44, C19orf55, and C10orf88) or whose subcellular localization was not previously assessed (CCDC57, WDR83, GIGYF1, LZTS2). CEP55 was also tested; its presence in our dataset was intriguing because it is a centrosome protein that also localizes to the midbody during cytokinesis and is required for cell cycle progression and cytokinesis (Martinez-Garay *et al*, 2006; Zhao *et al*, 2006). Several other polypeptides previously reported to localize to the midbody or regulate mitosis were also identified in our BioID analysis, *e.g.,* CYLD, SIRT2, CSPP, and SPAG5, the latter two being centriolar satellite components (Table EV3) (Gruber *et al*, 2002; Dryden *et al*, 2003; Patzke *et al*, 2005; Stegmeier *et al*, 2007; Thein *et al*, 2007; Inoue *et al*, 2009; Gomez-Ferreria *et al*, 2012).

The 11 centriolar satellite candidates were transiently expressed as FLAG-tagged fusion proteins in RPE-1 cells, and immunostaining was conducted for the FLAG tag, satellite, and centriole markers. Of the four genes chosen from the core, CCDC138, CEP55, and CCDC22 are *bona fide* satellite-resident proteins (Fig 2C), displaying an IF signal that overlaps with PCM1 in interphase cells. Of the seven candidates with a lower indegree (Fig 2B), two proteins (CCDC57 and CCDC92) partially colocalized with PCM1, indicating that they are also satellite proteins (Fig 2C). In addition to its localization to centriolar satellites, CCDC92 was previously shown to interact with and colocalize with CEP164 at the mother centriole (Chaki *et al*, 2012). In summary, a partial survey of our satellite interaction landscape identified five novel satellite components, suggesting that further mining of this proteome will yield additional centriolar satellite constituents.

Prey–prey correlation analysis reveals novel interaction signatures

Prey proteins that display similar interaction signatures are likely to colocalize and/or function together. Prey-centric analysis can thus be an informative approach for assessing large proteomes (Youn *et al*, 2018). To gain further insight into the composition and function of centriolar satellites, we performed a number of correlation and clustering analyses on the satellite dataset, as previously described (Knight *et al*, 2017). To refine the specific clusters identified by the 22 satellite baits used in this study, we merged these data with the related centrosome–cilia BioID dataset, composed of 58 baits in a similar biological context (Gupta *et al*, 2015) and visualized the correlation data as a prey–prey heat map (Figs 3A and EV3A and Table EV5). This analysis revealed a strong signature that was significantly enriched for satellite and centrosome proteins (GO:0005813; centrosome; $P = 10^{-61}$) (Fig EV3A; see Materials and Methods).

A closer look at the prey-centric clustering map shows highly correlated prey signatures corresponding to a number of known protein complexes (Fig EV3A, green fonts, and several (underlined) are enlarged in Fig EV3B). For instance, we observed high prey–prey correlation values for two structural subunits of the protein phosphatase 2 (PP2), CP110 and CEP97, which are known to partner for centrosome–cilia function (Spektor *et al*, 2007); three subunits of the prefoldin complex, PFDN2, PFDN5, and PFDN6; five subunits of the dynactin complex (Fig EV3B, green fonts); and eight subunits of the HAUS complex (Fig EV3A and B, green branch and fonts). Large prey signatures corresponded to interactions with components of the ER and Golgi (Fig EV3A), and interestingly, there is an additional signature comprising components of the P-body (GO:0000932; $P = 10^{-14}$, Fig EV3B). Notably, this analysis also clustered (Fig 3B, purple fonts and branch) the two known satellite components C11orf49 and LRRC49 with the uncharacterized protein TPGS1 (Figs 3B and EV3C). TPGS1 is the putative human homolog of the murine tubulin polyglutamylase subunit 1 (Tpgs1), which localizes to centrioles in mouse embryonic cells (Regnard *et al*, 2003). Consistent with the high prey–prey correlation value shared with two known satellite components, human GFP-TPGS1 displayed robust colocalization with PCM1, indicating that it is also a *bona fide* satellite component (Fig 3C). To further substantiate this finding and to reveal its proximal interactome, we tagged TPGS1 with BirA*-FLAG, confirmed its localization and biotinylation by IF and Western blot (WB) (Fig 3D–E), and subjected it to BioID. As a result, 55 high-confidence interactors, 23 of which are known satellite proteins (Fig 3F and Table EV6), were identified. Notably, we did not identify any new high-confidence hits not already found in the interactome of the other 22 satellite baits, suggesting that in its current form, the satellite proteome in HEK293 cells is near saturation. We validated five of these interactions using co-immunoprecipitation (co-IP; Fig 3G), confirming that TPGS1 is a satellite protein. Thus, our prey-centric correlation approach validates known interactions among satellite and centrosome components, and can be utilized to discover new interactors of varied biological functions.

Microscopic and proteomic profiling of centriolar satellites reveals discernable populations

To gain insight into interactions among satellite proteins, we compared the pattern of interaction of satellite preys with that of PCM1 (Dammermann & Merdes, 2002) (red arrow row in Fig 3A; selected satellite genes enlarged in Appendix Fig S4A). The resulting correlation coefficients display a relatively large range of values ($r^2 = 0.13–0.85$; Fig 4A), indicating that significant differences exist between the association profiles of satellite prey proteins. To examine whether this difference in association profiles was reflected at the subcellular localization level, we utilized an automated low- to super-resolution imaging pipeline to generate colocalization indices of satellite proteins with respect to PCM1 (Fig 4B; see Materials and Methods). Briefly, cycling RPE-1 cells were fixed and labeled with antibodies directed against endogenous PCM1 and a second satellite protein. Isolated cells were identified by low-resolution scanning followed by image analysis and then reimaged using 3D structured illumination microscopy (3D-SIM). The colocalization mask was generated from a merge of both labeling patterns, and the correlation of intensities (for the two satellite proteins in these masked regions) was quantified and averaged per cell (Fig 4B). The higher resolution imaging allows us to resolve individual satellites within larger satellite groups in the vicinity of the centrosome, which is difficult to do using widefield microscopy and allows for more precise quantification (Appendix Fig S4B).

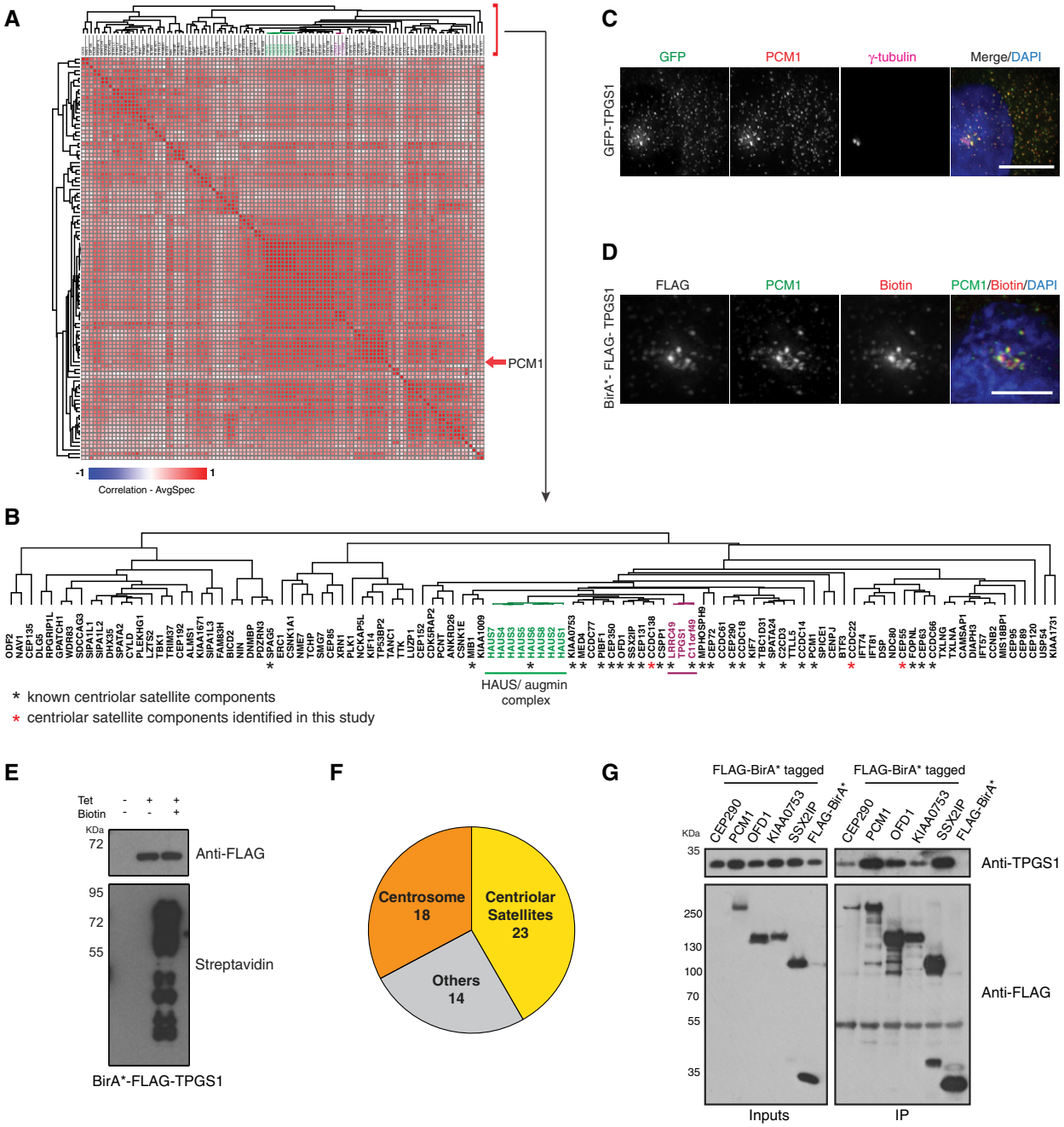

Figure 3. TPGS1, a new satellite protein found through prey–prey correlation analysis.

A Correlation matrix and associated dendrogram created from the centrosome cluster of Fig EV3A using Gene-E (details in Materials and Methods). Red arrow indicates location of PCM1 (zoomed in Appendix Fig S4A).

B Dendrogram of the centrosome clustering results in (A). The HAUS complex (green) and TPGS1 cluster (purple) are highlighted. Black asterisks indicate known satellite components, and red asterisks indicate novel satellite proteins identified in this study (Fig 2C).

C hTERT RPE-1 cells stably expressing GFP-TPGS1 were immunostained with antibodies directed against GFP, PCM1 (for satellites), γ-tubulin (for centrosome), and DAPI. Scale bar, 5 μm.

D Flp-In T-REx 293 cells stably expressing Tet-inducible BirA*-FLAG-tagged TPGS1 were fixed 24 h after induction. Cells were stained with the indicated antibodies, Alexa Fluor 594-coupled streptavidin for biotinylated proteins, and DAPI for nucleus. Scale bar, 5 μm.

E Western blots demonstrating tetracycline-inducible protein expression (anti-Flag, top) and biotinylation of proximal proteins (streptavidin-HRP, bottom) for BirA*-FLAG-TPGS1.

F Distribution of TPGS1 preys identified using BioID. TPGS1 yielded proximity interactions with 55 high-confidence preys, 31 of which are known satellite and/or centrosome proteins (see Table EV6 for the full list of interactors).

G A subset of TPGS1 proximity interactors were validated by co-IP. Flag pulldowns conducted on whole cell lysates of HEK293 cells expressing FLAG-BirA*-tagged CEP290, PCM1, OFD1, KIAA0753, or SSX2IP (or FLAG-BirA* alone as a negative control) were subjected to immunoprecipitation using anti-FLAG beads. Input supernatants and the IP material were separated via SDS–PAGE and immunoblotted using the indicated antibodies.

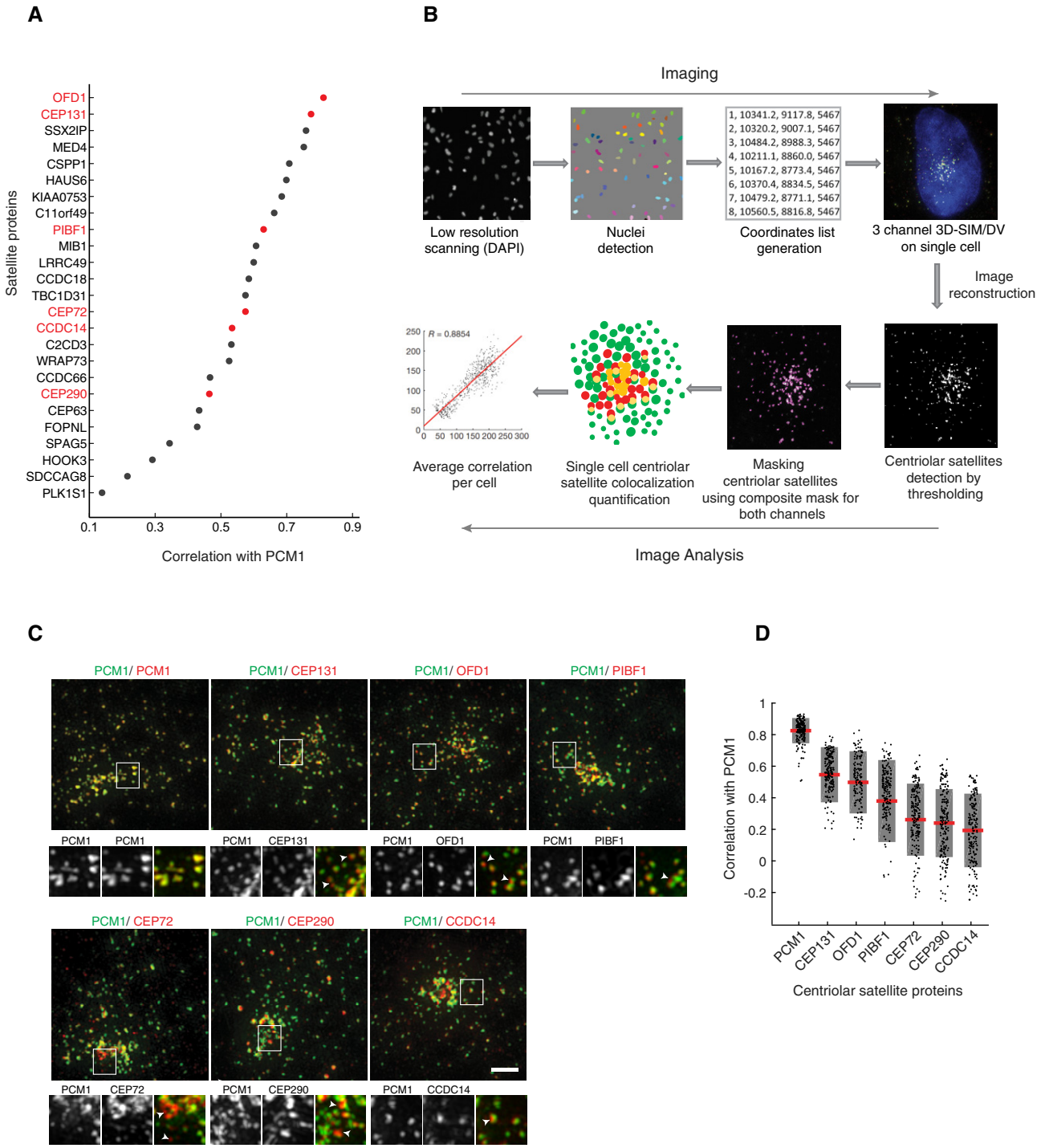

Figure 4. Satellite proteins display a ranked correlation of colocalization with PCM1.

A The correlation coefficient of several satellite bait proteins with PCM1 was extracted from the prey–prey clustering (Fig 3A red arrow, also enlarged in Appendix Fig S4A). Protein names highlighted in red were selected for further localization analysis presented in (C).

B Schematic of the low- to super-resolution microscopy pipeline used to analyze satellite protein localization (see Materials and Methods for details).

C hTERT RPE-1 cells were fixed with methanol and stained for PCM1 (green) and the indicated satellite marker (red). Two secondary antibodies labeled with different fluorophores were used to label PCM1 in both channels as control (top left panel). Samples were imaged using a 3D-SIM super-resolution microscope (OMX). White boxes represent the zoomed-in regions, and the white arrowheads highlight examples of the satellite structures with reduced PCM1. See Appendix Fig S4C and D for more details. Scale bar, 3 μm. Note that the pixel size in the 3D-SIM is half the size (0.04 μm) of the widefield (0.08 μm).

D Box-and-whisker plot showing the two-channel intensity correlation of pixels corresponding to regions identified with PCM1 and a second satellite marker (N = 200 cells per condition). Red lines indicate the average, and gray bars indicate SD.

We chose a subset of the known satellite proteins covering a range of prey correlations (marked in red in Fig 4A). The colocalization index of PCM1 labeled with a single primary antibody, and secondary antibodies coupled to two different fluorophores, was used as a control (Fig 4C). Consistent with their similarity in interacting partners (Fig 4A), CEP131 and OFD1 displayed high colocalization coefficients with PCM1 (Fig 4D). For PIBF1, CEP72, CEP290, and CCDC14, the lower level of prey profile correlations coincided with lower colocalization indices.

To rule out the possibility that the signal from satellite proteins at or in the vicinity of the centrosome would skew our intensity correlation profiling, we also performed the same analysis while excluding the centrosome region. Our analysis revealed that using this method, ~10–20% of the total signal was lost with some variation depending on the centriolar satellite protein analyzed (Appendix Fig S4C and Appendix Methods). This analysis led to a predictable decrease in intensity correlation overall, but nonetheless, the general trend previously observed was maintained (*e.g.*, PCM1/CEP131 signals correlate much more than PCM1/CEP290) (Appendix Fig S4D and Appendix Methods). Therefore, the colocalization of satellite components with PCM1 appears to reflect their interaction profiles suggesting diversity in satellite composition.

Perturbing PCM1 function alters the cellular distribution and proximity interaction profiles of centriolar satellite proteins

To investigate the effect of PCM1 loss on the other satellite components, we disrupted the *PCM1* gene in RPE-1 Cas9 cells using the CRISPR/Cas9 system (see Materials and Methods). Efficiency of the guide targeting PCM1 was assessed using TIDE (Tracking of Indels by DEcomposition) analysis following genomic PCR and sequencing of mixed pools of cells prior to selecting single clones (Appendix Fig S5A and B). PCM1 signal was absent in PCM1-depleted cells, as assessed by both IF and WB (Fig EV4A and Appendix Fig S5C). The distribution of CEP131, PIBF1, CEP72, OFD1, and CEP290 was restricted to the immediate vicinity of the centrosomes (Fig EV4A), indicative of satellite loss and in agreement with previous studies (Hoang-Minh *et al*, 2016; Wang *et al*, 2016; Odabasi *et al*, 2019).

To investigate whether PCM1 disruption alters the centriolar satellite proximity interaction landscape, we used the same CRISPR/Cas9 strategy to disrupt the *PCM1* gene in five HEK293-inducible cell lines (FLAG-BirA*-tagged CCDC66, CCDC14, PIBF1, and TEX9 and in cells expressing FLAG-BirA* only; see Materials and Methods). PCM1 depletion was confirmed by WB and IF (Figs 5A and B, and EV4B and C). In contrast to RPE-1 cells, we were not able to fully knock out PCM1 in HEK293 cells, but achieved an appreciable decrease in PCM1 protein levels, to 10% or less of that observed in WT cells (Fig EV4B). Importantly, IF analyses indicated that PCM1 localization to satellite-like structures was dramatically reduced in each of the HEK293 PCM1-depleted lines, similar to what we observed in the RPE-1 PCM1 KO cells, and biotinylated product localization was restricted to the immediate vicinity of centrosomes, consistent with satellite loss (Figs 5B and EV4C). However, in line with our WB results, and in contrast with the RPE-1 PCM1 KO, a fraction of HEK293 cells with seemingly intact satellites could still be observed, likely due to cell-to-cell heterogeneity in this cell line. BioID identified 207 high-confidence interactors (444 PxIs) in PCM1 WT vs. 152 high-confidence interactors (281 PxIs) in the PCM1-depleted cell lines (Table EV7 and Fig 5C). Data-driven topological networks for this four bait dataset and data for individual baits are displayed in Fig 5C and D, respectively.

Among the 84 core satellite proteins defined by the 22 baits in WT HEK293 cells (circled in Fig 1C), 82 were detected by at least one of the four baits characterized in PCM1-depleted HEK293 cells. However, consistent with satellite disruption in PCM1-depleted cells, bait–prey clustering highlighted a number of lost bait–prey interactions (Fig 5E, orange and red boxes). For example, CEP72 and C2CD3 are lost as preys in all four baits following PCM1 depletion. Other satellite preys such as CCDC18, PIBF1, or CCDC14 were lost by at least two baits. Interestingly, however, while the satellite structures are missing in most cells, many of the underlying protein–protein interactions were maintained (Fig 5E, white boxes). Several different subgroups of proteins that are either known to function together (*e.g.*, Group 1, CCP110, and CEP97) or which display similarities in their interaction patterns (*i.e.*, share a similar pattern of prey protein losses in PCM1-depleted cells) were manually annotated. These groups are likely to represent functional protein modules, since they maintain proximity interactions even in the absence of intact centriolar satellites (Fig 5E, circled numbers). Interaction profiles of these modules are presented in Fig 5F.

The proximity interaction landscape of satellites is maintained in the absence of centrioles

While it is well established that satellites participate in the biogenesis of centrioles via the delivery of centriole proteins to the site of centriole assembly, the role of centrioles/centrosomes in the maintenance of satellite integrity is much less clear. To investigate the relationship between centrioles and satellite organization, we depleted centrosomes from cells using prolonged centrinone treatment, which gradually depletes centrioles via inhibition of Polo-like kinase 4 (PLK4), a regulator of centriole duplication (Wong *et al*, 2015). Centriole loss normally leads to a p53-dependent G1 arrest (Bazzi & Anderson, 2014; Meitinger *et al*, 2016). Due to their immortalization by adenoviral proteins (Ad5 E1A and E1B), HEK293 cells lack normal p53 function (Martin & Berk, 1998) and cycle normally in the absence of centrioles. Thus, after 7 days of centrinone treatment, ~60% of HEK293 cells lacked centrioles (Fig 6A and B).

We observed that centrosome depletion in the centrinone-treated cells resulted in less pronounced MT organization (Fig EV5A), in a manner comparable to the elimination of centrioles via laser ablation (Khodjakov *et al*, 2000). Centriole-free cells also displayed more random MT arrays (Fig EV5A) nucleated from other organelles such as the Golgi apparatus or the nuclear envelope (Luders & Stearns, 2007; Maia *et al*, 2013). As previously shown in RPE-1 and U-2 OS cells, satellites, typically clustered around centrioles, are more dispersed in the cytoplasm upon centriole loss (Figs 6A and EV5A). Satellite dispersion was not caused by a change in satellite protein expression levels (Fig EV5C), indicating that satellites remain intact in the absence of centrioles and functional MT organizing centers (MTOCs).

To determine whether centriole depletion affects the satellite proximity interaction landscape, we performed BioID on seven satellite baits in cells treated with centrinone and depleted of centrioles (Fig 6C). These seven satellite baits yielded 306 (628 PxIs) and 368 (710 PxIs) high-confidence interactors in vehicle-treated (DMSO)

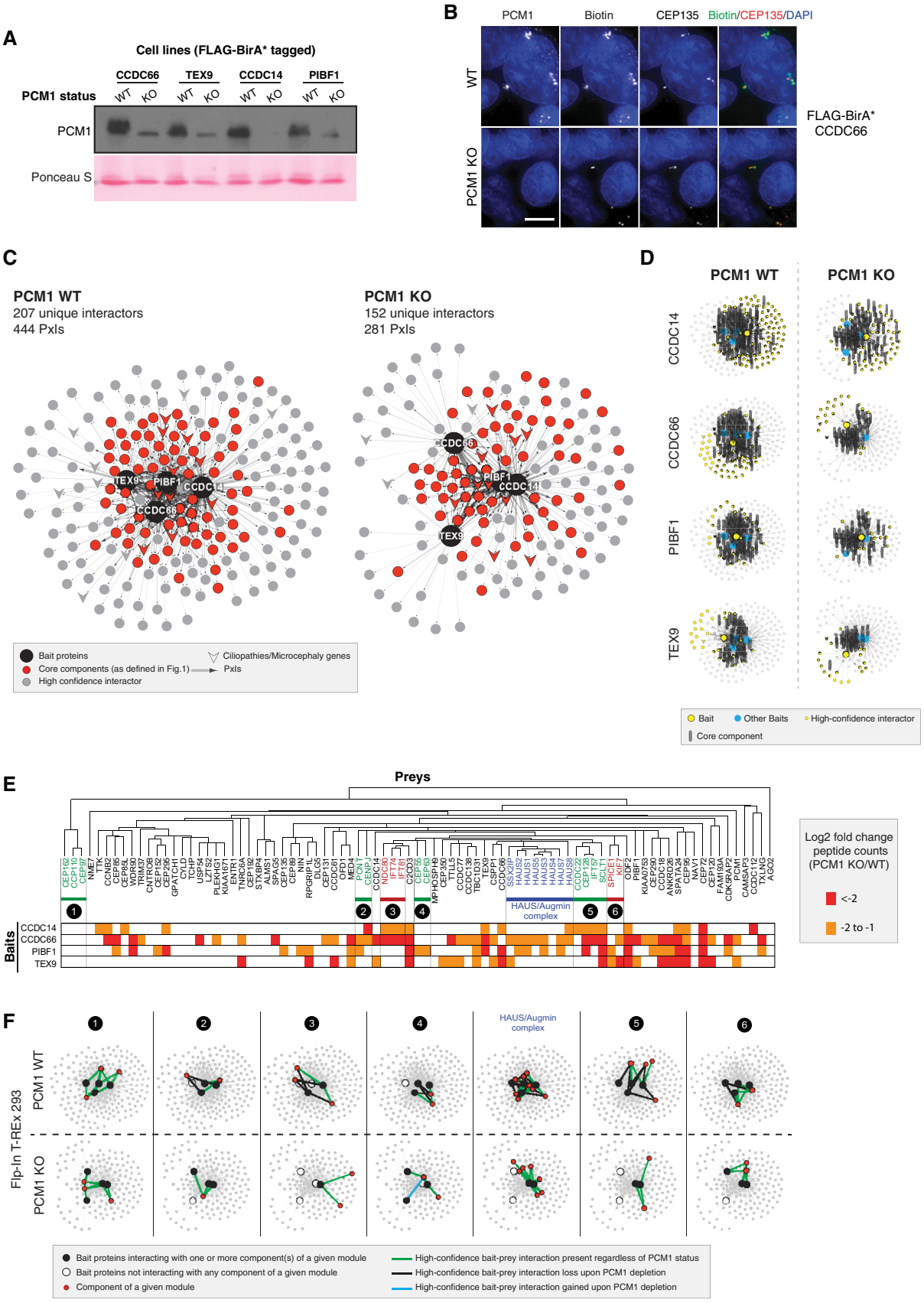

Figure 5.

Figure 5. Comparing the proximity interaction landscape of centriolar satellites in WT vs. PCM1 KO cell lines.

A WB indicating PCM1 protein expression levels in WT versus PCM1 KO HEK293 cells expressing FLAG-BirA*-tagged CCDC66, TEX9, CCDC14, or PIBF1. Ponceau S red staining was used as the loading control. See Fig EV4B for additional analysis.

B FLAG-BirA*-tagged CCDC66 was expressed in HEK293 WT or PCM1 KO cells. Cells were fixed 24 h after Tet and biotin addition, and stained with the indicated antibodies, Alexa Fluor 594-coupled streptavidin, and DAPI. PCM1 KO lines are devoid of satellite structures, and the biotinylated satellite proteins are localized to centrosomes. See Fig EV4C for other baits. Scale bar, 10 μm.

C Data-driven interactome networks of CCDC14, CCDC66, PIBF1, and TEX9 identified in the presence (WT) or absence (KO) of PCM1.

D Thumbnails of subnetworks (C) depicting individual bait protein interactomes. Large yellow nodes highlight individual bait proteins; blue nodes indicate the location of the other three bait proteins analyzed here; vertical bars highlight high-confidence "core" interactors of each indicated bait (as defined in Fig 1C).

E Satellite core protein component cluster (top; based on the Spearman rank correlation of peptide counts across the 22 satellite bait proteins). Heat map (bottom) highlighting moderate (orange) to substantial (red) loss of interactions in indicated BioID experiments performed in PCM1 KO and WT cells. Six protein modules displaying similar behavior (i.e., loss/no change in bait interactions in response to PCM1 depletion) are indicated.

F Interaction profile of interactor modules (indicated in 5E), 1–6, and HAUS complex in the presence or absence of PCM1. Black nodes represent bait proteins interacting with one or more component(s) of a given module; white nodes indicate bait proteins not interacting with any component of the given module; red nodes highlight the prey components of a given module; green edges indicate high-confidence bait–prey interactions present regardless of PCM1 status; black edges highlight high-confidence bait–prey interactions lost upon PCM1 depletion; blue edges indicate high-confidence bait–prey interactions gained upon PCM1 depletion.

versus centrinone-treated cells, respectively. 85% (262/306) of the interactors were detected in both conditions (Fig 6E and Table EV8), and the proximity interaction landscape of the satellite baits tested was largely unaffected (Figs 6D and EV5D and Table EV9). In fact, none of the preys initially localized to the "core" region (dashed black circle) are lost upon treatment (out of 75 core prey proteins, 65 remain in the core after centriole loss and 10 move to the periphery). The molecular composition of the periphery was slightly more variable, with two-thirds (170/231) of the interactors being conserved between the two conditions. Thus, overall, the molecular topology of the satellite network is preserved after centrinone treatment, exhibiting a slight decrease of satellite interactors in the core (75 vs. 84 hits in core) and a modest expansion of peripheral interactions (Fig 6E and Table EV8).

As shown in Fig 6B vs. Fig EV5B, the efficiency of centriole depletion in HEK293 cells is lower than other cell lines (Wong *et al*, 2015). We attempted to increase the depletion efficiency by titrating centrinone concentrations (350, 500, 750, 1,000, and 1,500 nM) and increasing the treatment duration (up to 12 days), but even at the highest dose and longest treatment time, about 40% of the cells retained their centrioles. To confirm that satellites are still present, and their interactions are maintained in the context of more efficient centriole depletion, we used a U-2 OS cell line in which the centriole duplication factor STIL was disrupted using CRISPR/Cas9 (Appendix Fig S6A) (Liu *et al*, 2018). Staining for PCM1 and the other satellite markers revealed that centriolar satellite structures remain present in STIL KO cells, but they are now dispersed, with no accumulation in the perinuclear region (Appendix Fig S6B). To determine whether satellite protein interactions are altered in the absence of centrioles, we performed co-IP in STIL KO and WT U-2 OS cells transiently expressing FLAG-BirA* or FLAG-BirA*-PCM1 (Appendix Fig S6C and Appendix Methods section). Interactions between PCM1 and the satellite proteins tested (CEP131, OFD1, and CEP72) were still detected in the absence of centrioles (Appendix Fig S6D). Together, these observations are in agreement with our MS data, suggesting that the satellite proximity interaction landscape is largely unaffected in the absence of centrioles.

The association of PCM1 with other centriolar satellite proteins is not perturbed upon depolymerization of microtubules

Disruption of the MT network impairs satellite distribution (Dammermann & Merdes, 2002; Lopes *et al*, 2011). We sought to investigate whether MT depolymerization also affects satellite protein interactions. To this end, MTs were disrupted using nocodazole, co-IPs were performed, and the spatial distribution of satellites was analyzed using microscopic imaging on mock (DMSO)- and nocodazole-treated samples (Fig 7A–C).

Along with the nocodazole-treated samples, we also validated some of the interactions identified in the centrinone BioID experiment. To this end, we chose a subset of satellite proteins and performed co-IP using the FLAG-BirA*-PCM1 stable cell line in mock-, nocodazole-, or centrinone-treated samples. Interaction of PCM1 with the tested satellite components in the untreated condition has been previously reported (Kim *et al*, 2008; Kim & Rhee, 2011; Lopes *et al*, 2011; Staples *et al*, 2012; Kodani *et al*, 2015), and our data from both BioID and co-IP experiments confirm these observations (Fig 7B).

As shown in Fig 7B, nocodazole or centrinone treatment has no effect on the PCM1 co-IP of a number of satellite proteins (CEP290, CEP131, OFD1, CCDC14, PIBFI, and CEP72), validating the interactions detected by BioID under centrinone-treated conditions and indicating that the MT network is not necessary for the interactions between these satellite components and PCM1. Together, these data indicate that the assembly and composition of satellites are independent of the presence of a centrosome or an intact MT network.

Finally, to determine whether the maintained satellite interactions (Fig 7B) observed upon nocodazole and centrinone treatments are also reflected at the subcellular localization level, we measured colocalization indices of the same satellite proteins relative to PCM1 in control (DMSO) versus cells with a disrupted MT network (nocodazole-treated) or depleted centrioles (centrinone-treated; Fig 7A and C). Considering that the morphology of HEK293 cells is not ideal for high-resolution imaging and that centriole loss causes cells to arrest in G1 in a p53-dependent manner (Wong *et al*, 2015), we chose to use RPE-1-ΔTP53 cells (Zimmermann *et al*, 2018), which cycle normally under prolonged centrinone treatment. Efficient centriole loss in RPE-1-ΔTP53 cells was confirmed by CEP135 staining (Fig EV5A and B). MT network disruption and subsequent satellite dispersion were confirmed by α-tubulin and PCM1 staining in the same cell line after nocodazole treatment (Fig EV6A). Cells were labeled with antibodies against PCM1 (green) and one other satellite member (red), as well as γ-tubulin (magenta) to mark centrosomes (Figs 7C and EV6D). Primary antibodies to PCM1 alone labeled with two different fluorophore-tagged secondary antibodies were used as reference points and alignment control for imaging and analysis

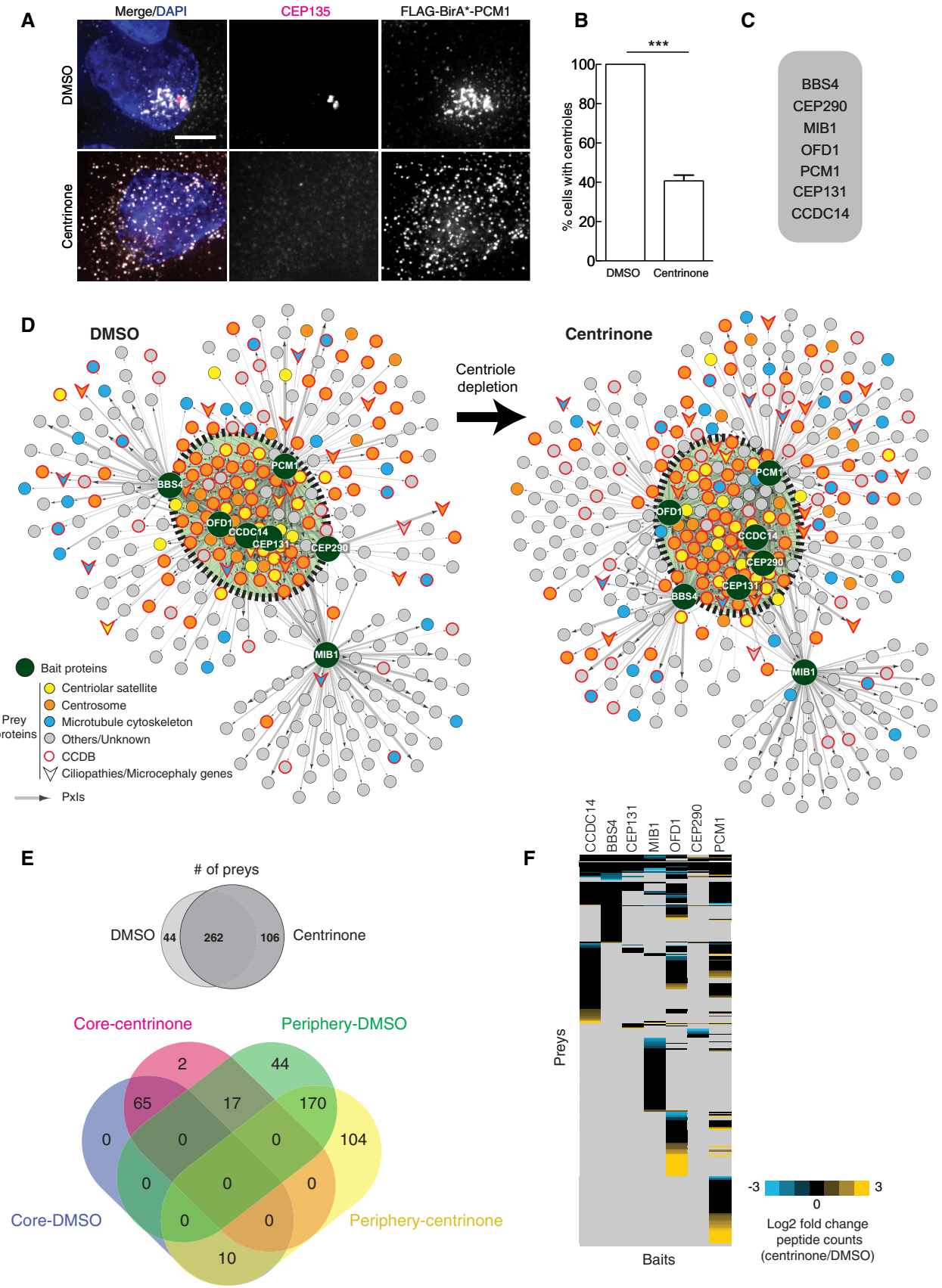

Figure 6.

Figure 6. Satellites disperse but their core interactome does not change upon centriole depletion.

A Flp-In T-REx 293 cells were treated with DMSO (control) or centrinone for 7 days, then methanol-fixed and stained with antibodies against FLAG and CEP135 (centrioles). In the centrinone-treated cells, centrioles are lost and the PCM1 marked satellites are dispersed. Scale bar, 5 μm.

B Cells (%) lacking centrioles based on micrographs in (A) (N = 300, three independent replicates (± SD), paired t-test, ***P = 0.0001).

C Baits subjected to BioID analysis in the centrinone experiment (see Table EV1 for more details).

D Self-organized interactome networks for the seven baits used to compare DMSO- and centrinone-treated (centriole less) cells. The black dashed circle delineates the "core" region.

E Venn diagrams indicating the number of high-confidence preys detected in each condition (top, gray), and the number of preys in the core vs. periphery in both conditions (bottom, color) (see Table EV8 for details).

F Heat map depicting log2 fold change (FC) peptide count ratio (centrinone/DMSO) of high-confidence interactors (in either condition). Log2 FC > 1 (yellow): prey proteins enriched by centrinone treatment. Log2 FC < −1 (blue): preys depleted by centrinone treatment. Log2 FC between −1 and 1 (black).

(Fig EV6B and C). Consistent with our co-IP and centrinone BioID data, the colocalization indices of PCM1 and the other satellite proteins were largely unchanged after each of the drug treatments (Fig 7D). A slight decrease was observed in some cases, which could be due to lower signal intensities following drug treatments. As expected, the subgroups that were defined based on our clustering and super-resolution imaging data (Fig 4) were reproduced in this experimental setting (Fig 7D). In summary, our data suggest that satellite integrity and assembly are largely independent of the presence of intact centrioles and MTs and that satellites retain the capacity to form spatially resolvable subpopulations.

Discussion

Using BioID to analyze 22 centriolar satellite baits, here we identified 2,113 interactions among 660 unique proteins. Due to the strength of BioID in capturing transient interactions, although this interactome is enriched in centrosome-related and MT-associated proteins, it also revealed other potential interactions with components of other cellular compartments (peripheral interactions, Fig 1C). Our dataset thus expands the number of satellite protein interactions by ~40%. Utilizing this network, we identified six novel satellite proteins, increasing the number of known satellite components (confirmed by cellular localization) to 50 (Table EV1). We anticipate that several yet uncharacterized proteins in the network are also likely to be satellite and/or centrosome proteins.

Using prey correlation profiling (Fig EV3A), we captured several known protein complexes and discovered novel subgroups that are likely to work together as functional modules (Fig 3B). As an example of how such an analysis could be exploited, we explored the TPGS1-containing cluster (Figs 3B and EV3C). Tubulin polyglutamylation is a post-translational modification important for centriolar stability and neuronal differentiation (Edde *et al*, 1990; Audebert *et al*, 1994; Bobinnec *et al*, 1998). Regnard *et al* (2003) purified the tubulin polyglutamylase (TPG) from mouse brain, demonstrating that it consists of at least three subunits from which they characterized PGs1 (Tpgs1), a conserved protein. They also showed that PGs1 has no catalytic activity but is important to localize the complex to sites of polyglutamylation. The same study demonstrated that GFP-PGs1 localized to centrosomes in mouse embryonic cells in a cell cycle- and MT-dependent manner similar to known satellite proteins. Here, we report that the human homolog TPGS1 clusters tightly with two known satellite proteins, LRRC49 and C11orf49 (Figs 3B and EV3C), and colocalizes with PCM1, confirming it as a new satellite component (Fig 3C–G). Our prey signature profile suggests that LRRC49 and C11orf49 comprise the other two subunits of the human TPG complex. Since centrioles are glutamylated (Bobinnec *et al*, 1998), and Tpgs1 is localized to the centriole (Regnard *et al*, 2003), we suggest that TPGS1 could play a role in transporting the polyglutamylase complex to centrioles. Interestingly, our network also contains other tubulin polyglutamylases, such as TTLL1 and TTLL5 (Janke *et al*, 2005), reinforcing a potential link between satellites and tubulin modifications.

Both our bait–prey and prey-centric correlation analyses shed light on the potentially undefined roles for satellites in association with other organelles or protein complexes of varied function. One such example is the GW/P-body components identified in our dataset (Figs EV2 and EV3B). There is evidence to support the association between RNA biology and centrosome-related processes. First, two GW/P-body proteins, AGO2 and GW182, localize to centrioles and basal bodies of ciliated human primary astrocytes. Interestingly, depleting either of these proteins affected ciliation (Aizer *et al*, 2008; Moser *et al*, 2011). Second, centrosomal RNA (CnRNA) has been detected on centrosomes of the surf clam (*Spisula solidissima*) (Alliegro, Alliegro *et al*, 2006; Chichinadze *et al*, 2013). Third, both satellites and a subgroup of P-body proteins have been shown to move along MTs (Dammermann & Merdes, 2002; Aizer *et al*, 2008). Finally, a recent BioID-based study on RNA bodies identified the centrosomal protein CEP85, a regulator of centriole duplication and PLK4 activity (Liu *et al*, 2018), as a high-confidence prey for multiple P-body baits. These observations suggest that satellites and centrosomes may play a yet undescribed role related to RNA processing and decay.

A recent study demonstrated that DYRK3, a dual specificity kinase known for regulating the stability of P-bodies (Wippich *et al*, 2013), interacts with multiple components of the centrosome/pericentriolar material, including PCM1 (Rai *et al*, 2018). Interestingly, inhibiting DYRK3 in mitotic cells results in aberrant condensation of PCM1 and stress granules. DYRK3 acts as dissolvase on multiple membraneless organelles during mitosis, including centriolar satellites (Rai *et al*, 2018). Under the conditions used in this study, DYRK3 was not detected as a satellite interactor, which may be due to the relatively low level of expression of this protein in HEK293 cells. It will be interesting to determine whether preferential association with satellite components is more robustly observed in mitosis or under cellular stress.

Our prey-centered clustering also indicated that satellites are closely associated with all eight subunits of the HAUS complex (Figs 3B and EV3A). HAUS localizes to interphase centrosomes and the spindle MT and is the counterpart of the *Drosophila* Augmin

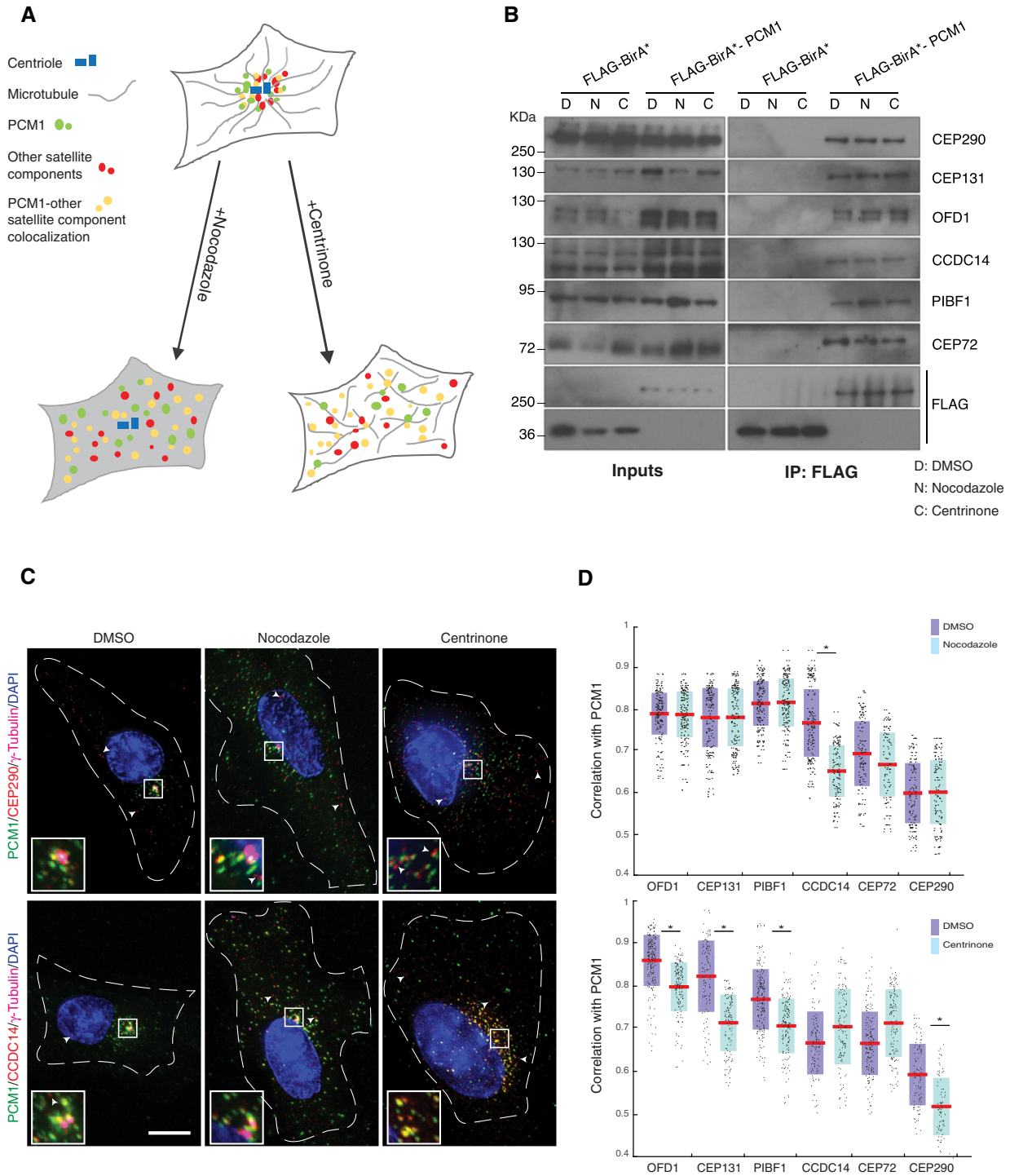

Figure 7. Satellite interactome and colocalization with PCM1 are independent of centrioles and microtubules.

A Schematic representation of the drug treatments used before imaging and colocalization analysis. Satellites disperse following centrinone or nocodazole treatment.

B Co-IP demonstrates interactions between PCM1 and several satellite components. HEK293 cell lines stably expressing FLAG-BirA* alone or FLAG-BirA*-PCM1 were subjected to DMSO (control), nocodazole, or centrinone treatment. Cell lysates were immunoprecipitated with anti-FLAG beads. Input and IPs blotted as indicated. Anti-FLAG detects FLAG-BirA* (~36kDa) in the control cell line and FLAG-BirA*-tagged PCM1 (~300kDa) in the FLAG-BirA*-PCM1 cell line.

C RPE-1-ΔTP53 cells were treated with DMSO (control), centrinone (7 days), or nocodazole (3 h), fixed with methanol and stained with antibodies directed against PCM1 (green), CEP290 or CCDC14 (red), γ-tubulin (purple) to mark the centrosome, and DAPI (blue). Note dispersed satellites in nocodazole- and centrinone-treated cells. White arrowheads highlight examples of the satellite structures that lack PCM1. Individual channels are shown in Fig EV6D. Scale bar, 10 μm.

D Box-and-whisker plots displaying the coefficient of correlation of colocalization with PCM1 (N~150 cells per condition) under the indicated conditions. Red lines indicate the average, and the purple or blue bars indicate SD. Two-tailed t-test, $^*P = 0.02$.

complex (Goshima *et al*, 2008). HAUS is important for stabilizing kinetochore MTs, and its depletion leads to a kinetochore MT defect and a decrease in spindle MT density. The close association of HAUS and satellite components, and HAUS6 localization to satellites (Gupta *et al*, 2015) suggest that satellites could play a role in transporting the subunits or homeostasis of the HAUS complex. Further studies are required to assess the molecular mechanisms of the interactions between satellites and HAUS.

Satellites are known to be dynamic structures shuttling on MTs both toward and away from the centrosomes. This movement is dependent on MTs and a dynein–dynactin motor complex (Balczon *et al*, 1999; Kubo *et al*, 1999; Dammermann & Merdes, 2002). Dynein is a minus-end-directed motor that moves the satellites toward the centrosome. To move away from the centrosome, satellites would need to travel via kinesins, the plus-end-directed motors. Multiple dynactin and cytoplasmic dynein subunits were detected in our BioID analysis (Fig EV3A and B), along with a number of plus-end-directed kinesin motor proteins. Indeed, KIF7, KIF14, KIF2C, and KIF20A were among our high-confidence hits, making them potential candidates for moving satellites away from the centrosome.

Based on the growing number of satellite constituents, their wide range of activities, and our clustering and correlation data (Fig 4), individual satellites are likely to be composed of different subgroups of proteins to serve different functions. This has been alluded to previously (Kodani *et al*, 2015), but the proteomics and satellite groups we have defined here are the first direct demonstration of this. Based on varying levels of colocalization between PCM1 and other satellite proteins, we can speculate that PCM1 is present only on a subset of centriolar satellite structures. Another possibility could be that PCM1 associates more transiently with some populations of centriolar satellites, which leads to a steady-state distribution predominantly to specific subpopulations. We also find that some satellite proteins also localize to centrosomes and other subcellular structures, which highlights the potential interplay between distinct centriolar satellite populations and other cellular functions. Systematic functional profiling of the various satellite populations in diverse cellular readouts will allow this hypothesis to be thoroughly tested in the future. Interestingly, we have shown that satellites do not contain equal levels of PCM1 (Fig 4C and D), yet all satellites appear to be sensitive to PCM1 depletion (Wang *et al*, 2016; Odabasi *et al*, 2019). One possible explanation for these observations could be that PCM1 is necessary for the formation of centriolar satellite structures, but is not required for their maintenance, and could thus be lost over time. Alternatively, these observations could also be due to unappreciated dynamic properties of PCM1 that are difficult to capture in end-point assays such as those used in this study. More work will be required to address these questions.

To investigate the effect of PCM1 disruption on the centriolar satellite interactome, we knocked out *PCM1* in four of the satellite bait cell lines (FLAG-BirA*-tagged CCDC66, TEX9, CCDC14, and PIBF1) and performed BioID on them in parallel with their WT counterparts. As expected, the cells were devoid of satellites and the tested satellite markers were restricted to the centrosomes, as previously reported (Wang *et al*, 2016; Odabasi *et al*, 2019). Interestingly, even though satellites were disrupted, a large number of proximity interactions persisted, indicating that these protein complexes can either assemble in a PCM1-independent manner or that these interactions can also occur at the centrosomes. Precedent for this exists in the literature; for example, numerous proximity interactions of stress granule components are maintained in the absence of stress and despite dramatic changes in their cellular distribution (Youn *et al*, 2018). Similarly, analysis of the proximity interaction landscape of the centrosome–cilium interface in ciliated and non-ciliated cells demonstrated that the overall topology of the network is not dramatically altered in the absence/presence of cilia, although numerous interactions are gained in the ciliated state (Gupta *et al*, 2015).

To study the impact of centrosomes on satellite composition and assembly, we analyzed the proximity interactomes of seven satellite baits in cells with or without centrinone treatment. Centrinone prevents new centriole assembly by inhibiting PLK4, the master regulator of centriole duplication (Wong *et al*, 2015). As a result of the MTOC loss, MTs fail to focus at a single area and satellites are dispersed (Khodjakov *et al*, 2000). We found that after centrosome loss, the vast majority of satellite interactions are preserved, suggesting that their proteomic composition is largely independent of functioning centrosomes (Figs 6D–F and EV5D). Indeed, all preys that interact with five or more bait proteins are maintained after centriole loss. 86% of these preys remain in the core of the self-organized map, and the remainder move to the periphery. There is a gain of interactions in the network periphery, likely reflecting the change in subcellular localization that occurs upon satellite scattering. The fact that centriolar satellites contain so many centrosome–cilia-derived components in the absence of centrosomes is intriguing and suggests that self-assembly properties of their resident proteins drive their assembly.

To investigate protein interactions unique to satellites or centrosomes, we compared our previous dataset on the centrosome–cilium interface (Gupta *et al*, 2015) consisting of 31 centriole and centriolar appendages baits, with the satellite interactome generated in this study. We observed that 34.3% of interactions were also detected in the satellite interactome (Appendix Fig S7). Conversely, 39.9% of the satellite interactome overlaps with the centrosome dataset (Appendix Fig S7). Thus, while significant overlap is observed between the two interactomes, the majority of interactions appear to be specific to their respective interactome. Interestingly, the satellite "core" proteins did share more significant overlap with the centrosome interactome, suggesting that these highly connected proteins could play important roles in both organelles (Appendix Fig S7 and Table EV10). Strikingly, we observed that none of the 20 centriole and centriolar appendage baits previously profiled using BioID (Gupta *et al*, 2015) that are present as preys in our centriolar satellite dataset are lost in centrinone-treated cells, suggesting that proximal interactions between satellites and centriole components can still occur in the absence of centrioles. Further studies are needed to clarify the molecular mechanisms underlying these specific interactions and their role in satellite biogenesis and function. Furthermore, we found that even though satellites were disrupted, a large number of proximity interactions persisted, indicating that these protein complexes can either assemble in a PCM1-independent manner or that these interactions can also occur at centrosomes. Together, these data indicate that although these two organelles are vastly interconnected, a portion of the proximity interactions observed between their resident proteins are to some

degree independent of each other. It would be of great interest to unambiguously define compartment-specific components. We believe that satellites cannot be defined precisely based solely on the proximity interaction profiles of either satellite or centrosome components. Achieving this would require orthogonal methods (e.g., biochemical purification followed by mass spectrometry) or the use of more conventional affinity purification methods followed by mass spectrometry.

Overall, our observations raise the tantalizing possibility that satellite biogenesis is largely independent of the centrosome. One possibility is that satellite assembly depends mostly on the presence of intact microtubules or alternative MT nucleation centers (*e.g.*, the Golgi apparatus) (Petry & Vale, 2015; Kolobova *et al*, 2017). We find, however, that while satellites are dispersed upon disruption of the MT network, their interactions with PCM1 are maintained, suggesting that the MT network is not necessary for satellite assembly. Further studies will be required to fully understand the molecular mechanisms underpinning satellite biogenesis and function.

Materials and Methods

Cell culture and drug treatments

Flp-In T-REx 293 cells (Invitrogen) were grown in Dulbecco's modified Eagle's medium (DMEM) supplemented with 10% fetal bovine serum (FBS), GlutaMAX, zeocin (100 μg/ml), and blasticidin (3 μg/ml). Flp-In T-REx 293 stable lines expressing FLAG-BirA* or FLAG-BirA* fusion proteins were maintained as above, with the addition of hygromycin B (200 μg/ml) or puromycin (1 μg/ml). hTERT RPE-1 cells were grown in DMEM/F-12 supplemented with 10% FBS, GlutaMAX, and sodium bicarbonate (1.2 g/l). U-2 OS cells were cultured in McCoy's 5A medium with 10% FBS and GlutaMAX. All cells were cultured in a 5% CO_2 humidified atmosphere at 37°C. RPE-1-ΔTP53 cells were generated and maintained as detailed previously (Zimmermann *et al*, 2018).

To eliminate the centrioles, cells were grown in DMEM/F-12 complete media supplemented with 500 nM centrinone B (TOCRIS Biosciences) for 7 days. To disrupt the microtubules, 10 μM nocodazole (MilliporeSigma) was added to the medium for 3 h before fixing or harvesting. DMSO was used as control alongside the drug treatments.

Generation and characterization of Flp-In T-REx 293 pools for BioID

BioID (Roux *et al*, 2012) was carried out as described previously (Gupta *et al*, 2015). In brief, human full-length cDNA of the centriolar satellite baits was PCR-amplified from available constructs and cloned into the pcDNA5 FRT/TO FLAG-BirA* expression vector. Alternatively, the Gateway cloning system (using the BirA*-FLAG-tagged destination vector) was used whenever we had access to the Gateway entry clones through plasmid repositories. Using the Flp-In system, HEK293 cells stably expressing FLAG-BirA* (control) or FLAG-BirA*/BirA*-FLAG-tagged bait proteins were generated. After selection (DMEM + 10% FBS + 200 μg/ml hygromycin B or 1 μg/ml puromycin), 5 × 150 cm^2 plates of subconfluent (~70%) cells per biological replicate were incubated for 24 h in complete media supplemented with titrated level of tetracycline (Tet) (BioShop) (0.001–1 μg/ml) to avoid overexpression artifacts and 50 μM biotin (BioShop). Cells were collected and pelleted (1,000 rpm, 5 min), the pellet was washed twice with PBS, and dried pellets were snap-frozen.

For BioID in cells with depleted centrioles, HEK293 stable cell lines were grown in the presence of 500 nM centrinone B or DMSO (control), and Tet (1 μg/ml) for 7 days. 50 μM biotin was added on the sixth day for 24 h.

BioID sample preparation for MS

The BioID sample preparations were done essentially as described previously (Hua *et al*, 2017). Briefly, each cell pellet was resuspended in 10 mL of lysis buffer (50 mM Tris–HCl pH 7.5, 150 mM NaCl, 1 mM EDTA, 1 mM EGTA, 1% Triton X-100, 0.1% SDS, 1:500 protease inhibitor cocktail (Sigma-Aldrich), 1:1,000 benzonase nuclease (Novagen)), incubated on an end-over-end rotator at 4°C for 1 h, briefly sonicated to disrupt any visible aggregates, and then centrifuged at 45,000 *g* for 30 min at 4°C. The supernatant was transferred to a fresh 15-ml conical tube. 30 μl of packed, pre-equilibrated streptavidin sepharose beads (GE Healthcare) was added, and the mixture was incubated for 3 h at 4°C with end-over-end rotation. Beads were pelleted by centrifugation at 820 *g* for 2 min and transferred with 1 ml of lysis buffer to a fresh Eppendorf tube. Beads were washed once with 1 ml lysis buffer and twice with 1 ml of 50 mM ammonium bicarbonate (pH 8.3). Beads were transferred in ammonium bicarbonate to a fresh centrifuge tube, and washed two more times with 1 mL ammonium bicarbonate buffer. Tryptic digestion was performed by incubating the beads with 1 μg MS-grade TPCK trypsin (Promega, Madison, WI) dissolved in 200 μl of 50 mM ammonium bicarbonate (pH 8.3) overnight at 37°C. The following morning, 0.5 μg MS-grade TPCK trypsin was added, and beads were incubated 2 additional h at 37°C. Beads were pelleted by centrifugation at 2,000 *g* for 2 min, and the supernatant was transferred to a fresh Eppendorf tube. Beads were washed twice with 150 μl of 50 mM ammonium bicarbonate, and these washes were pooled with the first eluate. The sample was lyophilized and resuspended in buffer A (0.1% formic acid). $1/5^{th}$ of the sample was analyzed per MS run.

Mass spectrometry

MS/MS was done as previously described (Hua *et al*, 2017). Briefly, high-performance liquid chromatography was conducted using a 2 cm pre-column (Acclaim PepMap, 50 mm × 100 μm inner diameter (ID)) and 50 cm analytical column (Acclaim PepMap, 500 mm × 75 μm diameter, C18, 2 μm, 100 Å; Thermo Fisher Scientific, Waltham, MA), running a 120-min reversed-phase buffer gradient at 225 nl/min on a Proxeon EASY-nLC 1000 pump in-line with a Thermo Q Exactive HF Quadrupole-Orbitrap mass spectrometer. A parent ion scan was performed using a resolving power of 60,000, then up to the twenty most intense peaks were selected for MS/MS (minimum ion count of 1,000 for activation), using higher energy collision-induced dissociation (HCD) fragmentation. Dynamic exclusion was activated such that MS/MS of the same m/z (within a range of 10 ppm; exclusion list size = 500) detected twice within 5 s was excluded from analysis for 15 s. For protein identification, Thermo. RAW files were converted to the .mzXML format using ProteoWizard (Kessner *et al*, 2008), then searched using X!

Tandem (Craig & Beavis, 2004) and Comet (Eng *et al*, 2013) against the human Human RefSeq Version 45 database (containing 36,113 entries). Search parameters specified a parent ion mass tolerance of 10 ppm and an MS/MS fragment ion tolerance of 0.4 Da, with up to 2 missed cleavages allowed for trypsin. Variable modifications of +16@M and W, +32@M and W, +42@N terminus, and +1@N and Q were allowed. Proteins identified with an iProphet cutoff of 0.9 (corresponding to $\leq 1\%$ FDR) and at least two unique peptides were analyzed with SAINTexpress v.3.6.1 (Teo *et al*, 2014). Twenty control runs (from cells expressing the FLAG-BirA* epitope tag) were collapsed to the two highest spectral counts for each prey, and compared to the two technical replicates and two biological replicates of the bait BioID. High-confidence interactors were defined as those with BFDR ≤ 0.01 as described previously (Gupta *et al*, 2015).

Networks analysis

Self-organized interaction networks were generated using the "Perfuse Force Directed layout" (Cytoscape 3.6.1; iterations: 10,000; default node mass: 3; default spring length: 50; force-deterministic layout: on), with total spectral counts as the force parameter. Node and edge attributes have been assigned as indicated in the figure legends, and the resulting networks have been assembled in Illustrator satellites6 (Adobe). Base networks are available in supplemental data/website.

Data analysis and visualization tools

For generating the plots and maps, we used ProHits-viz as an online analysis and visualization tool (Knight *et al*, 2017; https://prohits-viz.lunenfeld.ca/). To make the dot plots shown in Figs 2B and EV2, the dot plot generator feature with the default options was used.

For generating Fig 3A, the entire SAINTexpress output files from the satellite proteome and the centrosome–cilia interface proteome (Gupta *et al*, 2015; Table EV5) were uploaded to ProHits-viz under the correlation analysis tab. Default settings were used for all parameters except the Avg. spec count used in the abundance column and the minimum bait requirement which was set as 2. The clusters labeled on the map and enlarged were obtained based on the enrichment terms calculated for the zoomed-in area using g:profiler with the dynamic viewer option.

The bait vs. bait scatter plots were made using the bait–bait comparison section of ProHits-viz. Both the primary and secondary filters were set at BFDR ≤ 0.01, and the data were transformed to log2. Color coding the satellites and labeling were done manually in Illustrator.

The dendrogram in Fig 3A was generated using the Gene-E software https://software.broadinstitute.org/GENE-E/. To do so, a similarity matrix with average spectrum was generated from the hits in the centrosome boxed area of Fig EV3A. Then, the correlation between the preys was calculated (one minus Pearson's correlation). The hierarchical clustering was then performed based on the prey–prey correlations.

GO analysis was performed using the ToppCluster tool (https://toppcluster.cchmc.org/), comparing side by side the enriched GO categories (MF, CC, and BP, and pathway) with a Bonferroni-adjusted cutoff *P*-value of 0.05. Table EV3 shows the −logP of the significantly enriched categories for each bait interactome and the corresponding high-confidence interactors assigned to each category for each bait protein (tab "All interactors", columns Z to AU).

To generate the bait–prey cluster in Fig 6F, the data have been clustered using Cluster 3.0, and preys and baits have been clustered by centroid linkage of the Spearman rank correlations as a similarity metrics. The heat map has been generated by Java TreeView (v 1.1.6r4).

Western blotting

Harvested cells were lysed in Laemmli buffer and treated with benzonase nuclease (MilliporeSigma). Proteins were separated via SDS–PAGE and transferred to PVDF membrane (GE Healthcare). Membranes were incubated overnight with the primary antibody in TBST (TBS, 0.1% Tween-20) with 5% skim milk powder (BioShop). For FLAG Western blots, the antibody solution was supplemented with 2.5% BSA Fraction V (OmniPur). After washing 3 × 10 min in TBST, the blots were incubated with secondary HRP-conjugated antibodies (Bio-Rad), then developed using SuperSignal chemiluminescent reagents (Thermo Scientific).

Co-immunoprecipitation

For co-immunoprecipitation of FLAG-BirA* fusions, one 10-cm dish of the respective HEK293 stable lines was incubated with Tet (1 μg/ml) for 24 h. After incubation, cells were washed with cold PBS and harvested. Cells were subsequently frozen at −80°C or lysed immediately in lysis buffer (50 mM HEPES pH 8, 100 mM KCl, 2 mM EDTA, 10% glycerol, 0.1% NP-40, 1 mM DTT, protease inhibitors (Roche)) for 30 min on ice. Lysates were frozen for 5 min on dry ice, then thawed and centrifuged for 20 min at 16,000 *g* at 4°C. Supernatants were incubated with anti-FLAG M2 affinity gel beads (MilliporeSigma) for a minimum of 3 h at 4°C (prior to incubation with beads, a fraction of supernatants (inputs) were saved). After incubation, beads were pelleted and washed with lysis buffer. Laemmli buffer was added, and samples (inputs and IPs) were boiled 5 min at 95°C in preparation for SDS–PAGE. Proteins were transferred to PVDF membranes and probed using anti-FLAG to detect the FLAG-BirA* fusions, and anti-TPGS1 or other satellite antibodies for the endogenous protein (antibodies listed in Table EV11).

For the co-IPs using drug-treated samples, FLAG-BirA* only and FLAG-BirA*-PCM1 cells were grown in the presence of Tet and centrinone or DMSO for 7 days, and then processed as described above. In the case of microtubule disruption, nocodazole was added to the Tet-induced cells 3 h before harvesting.

Generation of PCM1 KO lines

To generate hTERT RPE-1 PCM1 knockout (KO) cells, a gRNA (CTCTACAAGATCTTCCCGCA) targeting PCM1 exon 6 was selected from Hart *et al* (2015) and transcribed *in vitro* before being transfected into wild-type hTERT RPE-1 cells constitutively expressing Cas9 using Lipofectamine RNAiMAX (Invitrogen) according to the manufacturer's instructions. Approximately 5 days post-transfection, genomic DNA was purified, the target region was amplified by PCR, and the resulting product was sent for sequencing. Analysis by TIDE (Tracking of Indels by DEcomposition) allowed the efficiency

of the guide to be assessed using this website (https://tide.nki.nl/). The mixed pool of cells was plated such that single, clonal colonies could form. Following expansion, the clones were characterized and the indel in each was determined by genomic PCR and sequencing. The indel present in the selected clone was determined by genomic PCR and sequencing. Sequence alignment against wild-type confirmed the deletion of a single nucleotide in the guide region (Appendix Fig S5B). Downstream, this led to a premature stop codon, resulting in the protein of interest no longer being expressed which is further confirmed by WB (Appendix Fig S5C).

To disrupt PCM1 in four HEK293-inducible cell lines (FLAG-BirA*-tagged CCDC66, CCDC14, PIBF1, and TEX9), we used lentivirus-mediated CRISPR gene disruption. The guide RNA mentioned above was cloned into pLentiCRISPRv2 plasmid (Sanjana *et al*, 2014). Lentiviruses were produced in HEK293T cells using pCMV VSV-G and psPAX2 to package the viruses. Selected FLAG-BirA*-tagged bait cell lines (HEK293 background) were seeded in a 6-well plate and infected with varying amounts of virus and 8 μg/ml polybrene (MilliporeSigma). Media were changed after 24-h infection, and the selection media containing 1 μg/ml puromycin were added after 48 h. Cells from wells exhibiting ~50% survival after selection were characterized by WB and IF and were used for subsequent experiments.

Subcellular localization of tagged proteins

All 11 human genes tested in Fig 2B were cloned using the Gateway cloning system (Invitrogen) into pDEST 5′ 3xFLAG pcDNA5-FRT/TO following the manufacturer's instructions. Gateway entry clones were obtained from the open freezer plasmid repository at the Lunenfeld-Tanenbaum Research Institute (LTRI), and the Gateway parental vectors are available from the Gingras laboratory (http://gingraslab.lunenfeld.ca/resources.php?cateName=Reagents).

To generate GFP-TPGS1-expressing stable cell line, human TPGS1 cDNA was synthesized by GeneArt Invitrogen using the NM_033513.2 reference sequence from NCBI with the AscI and XhoI restriction site on the N and C terminus, respectively, and cloned into the pCMV-TO/FRT-Emerald (GFP) vector carrying a G418 resistance marker (Gupta *et al*, 2015).

hTERT RPE-1 cells were transfected with 1 μg of each plasmid using Lipofectamine 3000 (Invitrogen) following the manufacturer's protocol. Cells were fixed 24 h post-transfection for immunostaining. To generate the stable GFP-TPGS1 cell line, 48 h post-transfection, cells were selected with Geneticin (G418) (0.5 mg/ml).

Antibodies

A full list of the antibodies used in this study can be found in Table EV11.

Immunofluorescence microscopy

Cells were fixed for immunofluorescence with ice-cold methanol (10 min at −20°C), blocked with 0.2% fish skin gelatin (MilliporeSigma) in PBS (20 min at RT), and then incubated with primary antibody in blocking solution (1 h at RT). Following a washing step with blocking solution, cells were then incubated with fluorophore-conjugated secondary antibodies (Molecular Probes) and DAPI (0.1 μg/ml) in blocking solution (1 h at RT). After a final wash in blocking solution, coverslips were mounted onto glass slides by inverting them onto mounting solution (ProLong Gold Antifade, Molecular Probes). For the characterization of the HEK293 stable line expressing FLAG-BirA* fusion proteins, cells were additionally incubated with fluorophore-conjugated streptavidin (Molecular Probes). Cells were imaged using a DeltaVision Elite high-resolution imaging system equipped with a sCMOS 2,048 × 2,048 pixels^2 camera (GE Healthcare). Z-stacks (0.2 μm) were collected using a 60×/1.42 NA plan apochromat oil-immersion objective (Olympus) and deconvolved using softWoRx (v6.0, GE). The images are shown as maximum intensity projections (pixel size 0.1064 μm).

Super-resolution microscopy

Super-resolution imaging was performed as previously described (Mojarad *et al*, 2017). Briefly, cells were imaged on a three-dimensional (3D) structured illumination microscope (OMX Blaze v, GE) equipped with 405 nm, 488 nm, 568 nm, and 642 nm diode lasers, 4 high-speed sCMOS cameras (scientific CMOS, 2,560 × 2,560 pixels^2, manufactured by PCO), and a 60×/1.42 NA plan apochromat oil-immersion objective (Olympus). Multi-channel 3D-SIM image stacks (0.125 μm apart) were reconstructed and aligned, and maximum intensity was projected using the softWoRx 6.0 software package (GE). For high-throughput imaging, we developed a semi-automated imaging pipeline: First, a Python script was written to fuse adjacent, multi-z, wide-field images taken with the "mosaic" function in the imaging software; second, a Python script extracted the stage coordinates of the fused mosaic from the header of the combined image file; and third, a MATLAB script used a histogram-based threshold to detect single well-separated nuclei, calculated their position relative to the previously determined mosaic coordinates, and exported the point-of-interest coordinates to a softWoRx point list format. Super-resolution SI, 4-channel (405, 488, 568 and 608 nm), 512 × 512 pixel z-stacks were then automatically acquired, centered at each of the coordinates specified in the point list.

Colocalization analysis

All image quantifications were performed in MATLAB, and scripts can be provided upon request. Fields of cells were imaged using a 60× objective (NA 1.42, 2 × 2 binning). The coordinates of well-isolated single cells were then calculated and mapped into a point list. Images of single cells were then collected with automated or manual high-resolution widefield microscopy, or 3D-SIM. For 3D-SIM quantifications, we used reconstructed, maximum intensity projected, and aligned images. For widefield quantifications, we used deconvolved z-stacked images. For colocalization analyses, the centriole satellite mask was defined as the composite after detection of satellite regions (using constant signal-to-noise and size thresholds) in each image channel specific for the labeled centriolar satellite protein. Then, the intensities within the mask for each channel were compared with one another for every pixel, thereby generating a correlation coefficient (Lawo *et al*, 2012).

Note: Considering the satellite dispersion in the drug-treated sets (Fig 7C), the widefield microscopy is able to provide enough resolution for our analysis. We compared some of our super-resolution

images with their equivalent widefield ones, further confirming that the difference is negligible and will not affect our analysis (Appendix Fig S8).

Data availability

All mass spectrometry data have been deposited at the MassIVE data repository (massive.ucsd.edu ID: MSV000083121).

Expanded View for this article is available online.

Acknowledgements
We are grateful to J.Y. Youn, P. Samavarchi-Tehrani, A.C. Gingras, and J.D.R. Knight for advice on ProHits-viz and MS data analysis, and J. St-Germain for data deposition in MassIVE. We thank members of the Pelletier Lab for their scientific feedback during the project. We are grateful to J. Tkach and M.M. Aynaud for critically reviewing the manuscript and S. Cheung and K. Cormier for proofreading it. We thank R. Buijs for help generating U-2 OS STIL KO cells. RPE-1-ΔTP53 cells were a kind gift of M. Zimmermann and D. Durocher. We thank SciNet Consortium (http://www.scinethpc.ca/) of Compute Ontario (https://computeontario.ca) and Compute Canada (www.computecanada.ca) for their support. High- and super-resolution imaging was performed at the Network Biology Collaborative Centre (NBCC), a facility supported by Canada Foundation for Innovation, the Ontario Government, and Genome Canada and Ontario Genomics Institute (OGI-139). This work was funded by CIHR (MOP-142492) and the Krembil Foundation to L.P.

Author contributions
LG designed research and performed the experiments and analyses. EMNL carried out sample preparation for MS. EC, and BR performed the MS and the related analyses. GDG and MH developed the high-throughput super-resolution imaging pipeline. GDG performed image analyses. EC generated the Cytoscape networks. JG generated FLAG-BirA*-tagged C11orf49 and TBC1D31 stable cell lines. SLP generated the RPE-1 PCM1 KO cell line. LG, GDG, BR, and LP wrote the manuscript with input from all authors. BR and LP supervised and funded the project.

Conflict of interest
The authors declare that they have no conflict of interest.

References
Aizer A, Brody Y, Ler LW, Sonenberg N, Singer RH, Shav-Tal Y (2008) The dynamics of mammalian P body transport, assembly, and disassembly in vivo. *Mol Biol Cell* 19: 4154 – 4166

Alliegro MC, Alliegro MA, Palazzo RE (2006) Centrosome-associated RNA in surf clam oocytes. *Proc Natl Acad Sci USA* 103: 9034 – 9038

Alves-Cruzeiro JM, Nogales-Cadenas R, Pascual-Montano AD (2014) CentrosomeDB: a new generation of the centrosomal proteins database for Human and Drosophila melanogaster. *Nucleic Acids Res* 42: D430 – D436

Andersen JS, Wilkinson CJ, Mayor T, Mortensen P, Nigg EA, Mann M (2003) Proteomic characterization of the human centrosome by protein correlation profiling. *Nature* 426: 570 – 574

Audebert S, Koulakoff A, Berwald-Netter Y, Gros F, Denoulet P, Edde B (1994) Developmental regulation of polyglutamylated alpha- and beta-tubulin in mouse brain neurons. *J Cell Sci* 107(Pt. 8): 2313 – 2322

Balczon R, Bao L, Zimmer WE (1994) PCM-1, A 228-kD centrosome autoantigen with a distinct cell cycle distribution. *J Cell Biol* 124: 783 – 793

Balczon R, Varden CE, Schroer TA (1999) Role for microtubules in centrosome doubling in Chinese hamster ovary cells. *Cell Motil Cytoskelet* 42: 60 – 72

Barenz F, Inoue D, Yokoyama H, Tegha-Dunghu J, Freiss S, Draeger S, Mayilo D, Cado I, Merker S, Klinger M *et al* (2013) The centriolar satellite protein SSX2IP promotes centrosome maturation. *J Cell Biol* 202: 81 – 95

Barenz F, Mayilo D, Gruss OJ (2011) Centriolar satellites: busy orbits around the centrosome. *Eur J Cell Biol* 90: 983 – 989

Bazzi H, Anderson KV (2014) Acentriolar mitosis activates a p53-dependent apoptosis pathway in the mouse embryo. *Proc Natl Acad Sci USA* 111: E1491 – E1500

Bhogaraju S, Cajanek L, Fort C, Blisnick T, Weber K, Taschner M, Mizuno N, Lamla S, Bastin P, Nigg EA *et al* (2013) Molecular basis of tubulin transport within the cilium by IFT74 and IFT81. *Science* 341: 1009 – 1012

Bobinnec Y, Moudjou M, Fouquet JP, Desbruyeres E, Edde B, Bornens M (1998) Glutamylation of centriole and cytoplasmic tubulin in proliferating non-neuronal cells. *Cell Motil Cytoskelet* 39: 223 – 232

Chaki M, Airik R, Ghosh AK, Giles RH, Chen R, Slaats GG, Wang H, Hurd TW, Zhou W, Cluckey A *et al* (2012) Exome capture reveals ZNF423 and CEP164 mutations, linking renal ciliopathies to DNA damage response signaling. *Cell* 150: 533 – 548

Chichinadze K, Lazarashvili A, Tkemaladze J (2013) RNA in centrosomes: structure and possible functions. *Protoplasma* 250: 397 – 405

Comartin D, Gupta GD, Fussner E, Coyaud E, Hasegan M, Archinti M, Cheung SW, Pinchev D, Lawo S, Raught B *et al* (2013) CEP120 and SPICE1 cooperate with CPAP in centriole elongation. *Curr Biol* 23: 1360 – 1366

Conkar D, Culfa E, Odabasi E, Rauniyar N, Yates JR III, Firat-Karalar EN (2017) The centriolar satellite protein CCDC66 interacts with CEP290 and functions in cilium formation and trafficking. *J Cell Sci* 130: 1450 – 1462

Craig R, Beavis RC (2004) TANDEM: matching proteins with tandem mass spectra. *Bioinformatics* 20: 1466 – 1467

van Dam TJ, Wheway G, Slaats GG, Group SS, Huynen MA, Giles RH (2013) The SYSCILIA gold standard (SCGSv1) of known ciliary components and its applications within a systems biology consortium. *Cilia* 2: 7

Dammermann A, Merdes A (2002) Assembly of centrosomal proteins and microtubule organization depends on PCM-1. *J Cell Biol* 159: 255 – 266

Dryden SC, Nahhas FA, Nowak JE, Goustin AS, Tainsky MA (2003) Role for human SIRT2 NAD-dependent deacetylase activity in control of mitotic exit in the cell cycle. *Mol Cell Biol* 23: 3173 – 3185

Edde B, Rossier J, Le Caer JP, Desbruyeres E, Gros F, Denoulet P (1990) Posttranslational glutamylation of alpha-tubulin. *Science* 247: 83 – 85

Eng JK, Jahan TA, Hoopmann MR (2013) Comet: an open-source MS/MS sequence database search tool. *Proteomics* 13: 22 – 24

Farina F, Gaillard J, Guerin C, Coute Y, Sillibourne J, Blanchoin L, Thery M (2016) The centrosome is an actin-organizing centre. *Nat Cell Biol* 18: 65 – 75

Firat-Karalar EN, Rauniyar N, Yates JR III, Stearns T (2014) Proximity interactions among centrosome components identify regulators of centriole duplication. *Curr Biol* 24: 664 – 670

Firat-Karalar EN, Stearns T (2015) Probing mammalian centrosome structure using BioID proximity-dependent biotinylation. *Methods Cell Biol* 129: 153 – 170

Gomez-Ferreria MA, Bashkurov M, Mullin M, Gingras AC, Pelletier L (2012) CEP192 interacts physically and functionally with the K63-deubiquitinase CYLD to promote mitotic spindle assembly. *Cell Cycle* 11: 3555 – 3558

Goshima G, Mayer M, Zhang N, Stuurman N, Vale RD (2008) Augmin: a protein complex required for centrosome-independent microtubule generation within the spindle. *J Cell Biol* 181: 421 – 429

Gruber J, Harborth J, Schnabel J, Weber K, Hatzfeld M (2002) The mitotic-spindle-associated protein astrin is essential for progression through mitosis. *J Cell Sci* 115: 4053 – 4059

Gupta GD, Coyaud E, Goncalves J, Mojarad BA, Liu Y, Wu Q, Gheiratmand L, Comartin D, Tkach JM, Cheung SW *et al* (2015) A dynamic protein interaction landscape of the human centrosome-cilium interface. *Cell* 163: 1484 – 1499

Hart T, Chandrashekhar M, Aregger M, Steinhart Z, Brown KR, MacLeod G, Mis M, Zimmermann M, Fradet-Turcotte A, Sun S *et al* (2015) High-resolution crispr screens reveal fitness genes and genotype-specific cancer liabilities. *Cell* 163: 1515 – 1526

Hoang-Minh LB, Deleyrolle LP, Nakamura NS, Parker AK, Martuscello RT, Reynolds BA, Sarkisian MR (2016) PCM1 depletion inhibits glioblastoma cell ciliogenesis and increases cell death and sensitivity to temozolomide. *Transl Oncol* 9: 392 – 402

Hori A, Ikebe C, Tada M, Toda T (2014) Msd1/SSX2IP-dependent microtubule anchorage ensures spindle orientation and primary cilia formation. *EMBO Reports* 15: 175 – 184

Hori A, Toda T (2017) Regulation of centriolar satellite integrity and its physiology. *Cell Mol Life Sci* 74: 213 – 229

Hotokezaka Y, Katayama I, van Leyen K, Nakamura T (2015) GSK-3beta-dependent downregulation of gamma-taxilin and alphaNAC merge to regulate ER stress responses. *Cell Death Dis* 6: e1719

Hua R, Cheng D, Coyaud É, Freeman S, Di Pietro E, Wang Y, Vissa A, Yip CM, Fairn GD, Braverman N *et al* (2017) VAPs and ACBD5 tether peroxisomes to the ER for peroxisome maintenance and lipid homeostasis. *J Cell Biol* 216(2): 367 – 377

Inoue T, Nakayama Y, Yamada H, Li YC, Yamaguchi S, Osaki M, Kurimasa A, Hiratsuka M, Katoh M, Oshimura M (2009) SIRT2 downregulation confers resistance to microtubule inhibitors by prolonging chronic mitotic arrest. *Cell Cycle* 8: 1279 – 1291

Jakobsen L, Vanselow K, Skogs M, Toyoda Y, Lundberg E, Poser I, Falkenby LG, Bennetzen M, Westendorf J, Nigg EA *et al* (2011) Novel asymmetrically localizing components of human centrosomes identified by complementary proteomics methods. *EMBO J* 30: 1520 – 1535

Janke C, Rogowski K, Wloga D, Regnard C, Kajava AV, Strub JM, Temurak N, van Dijk J, Boucher D, van Dorsselaer A *et al* (2005) Tubulin polyglutamylase enzymes are members of the TTL domain protein family. *Science (New York. NY* 308: 1758 – 1762

Joachim J, Razi M, Judith D, Wirth M, Calamita E, Encheva V, Dynlacht BD, Snijders AP, O'Reilly N, Jefferies HBJ *et al* (2017) Centriolar satellites control GABARAP ubiquitination and GABARAP-mediated autophagy. *Curr Biol* 27: 2123 – 2136.e7

Kessner D, Chambers M, Burke R, Agus D, Mallick P (2008) ProteoWizard: open source software for rapid proteomics tools development. *Bioinformatics* 24: 2534 – 2536

Khodjakov A, Cole RW, Oakley BR, Rieder CL (2000) Centrosome-independent mitotic spindle formation in vertebrates. *Curr Biol* 10: 59 – 67

Kim J, Krishnaswami SR, Gleeson JG (2008) CEP290 interacts with the centriolar satellite component PCM-1 and is required for Rab8 localization to the primary cilium. *Hum Mol Genet* 17: 3796 – 3805

Kim K, Lee K, Rhee K (2012) CEP90 is required for the assembly and centrosomal accumulation of centriolar satellites, which is essential for primary cilia formation. *PLoS ONE* 7: e48196

Kim K, Rhee K (2011) The pericentriolar satellite protein CEP90 is crucial for integrity of the mitotic spindle pole. *J Cell Sci* 124: 338 – 347

Klinger M, Wang W, Kuhns S, Barenz F, Drager-Meurer S, Pereira G, Gruss OJ (2014) The novel centriolar satellite protein SSX2IP targets Cep290 to the ciliary transition zone. *Mol Biol Cell* 25: 495 – 507

Knight JDR, Choi H, Gupta GD, Pelletier L, Raught B, Nesvizhskii AI, Gingras AC (2017) ProHits-viz: a suite of web tools for visualizing interaction proteomics data. *Nat Methods* 14: 645 – 646

Kodani A, Tonthat V, Wu B, Sutterlin C (2010) Par6 alpha interacts with the dynactin subunit p150 Glued and is a critical regulator of centrosomal protein recruitment. *Mol Biol Cell* 21: 3376 – 3385

Kodani A, Yu TW, Johnson JR, Jayaraman D, Johnson TL, Al-Gazali L, Sztriha L, Partlow JN, Kim H, Krup AL *et al* (2015) Centriolar satellites assemble centrosomal microcephaly proteins to recruit CDK2 and promote centriole duplication. *eLife* 4: e07519

Kolobova E, Roland JT, Lapierre LA, Williams JA, Mason TA, Goldenring JR (2017) The C-terminal region of A-kinase anchor protein 350 (AKAP350A) enables formation of microtubule-nucleation centers and interacts with pericentriolar proteins. *J Biol Chem* 292: 20394 – 20409

Kubo A, Sasaki H, Yuba-Kubo A, Tsukita S, Shiina N (1999) Centriolar satellites: molecular characterization, ATP-dependent movement toward centrioles and possible involvement in ciliogenesis. *J Cell Biol* 147: 969 – 980

Kubo T, Brown JM, Bellve K, Craige B, Craft JM, Fogarty K, Lechtreck KF, Witman GB (2016) Together, the IFT81 and IFT74 N-termini form the main module for intraflagellar transport of tubulin. *J Cell Sci* 129: 2106 – 2119

Kwan J, Sczaniecka A, Heidary Arash E, Nguyen L, Chen CC, Ratkovic S, Klezovitch O, Attisano L, McNeill H, Emili A *et al* (2016) DLG5 connects cell polarity and Hippo signaling protein networks by linking PAR-1 with MST1/2. *Genes Dev* 30: 2696 – 2709

Lawo S, Bashkurov M, Mullin M, Ferreria MG, Kittler R, Habermann B, Tagliaferro A, Poser I, Hutchins JR, Hegemann B *et al* (2009) HAUS, the 8-subunit human Augmin complex, regulates centrosome and spindle integrity. *Curr Biol* 19: 816 – 826

Lawo S, Hasegan M, Gupta GD, Pelletier L (2012) Subdiffraction imaging of centrosomes reveals higher-order organizational features of pericentriolar material. *Nat Cell Biol* 14: 1148 – 1158

Lee GS, He Y, Dougherty EJ, Jimenez-Movilla M, Avella M, Grullon S, Sharlin DS, Guo C, Blackford JA Jr, Awasthi S *et al* (2013) Disruption of Ttll5/stamp gene (tubulin tyrosine ligase-like protein 5/SRC-1 and TIF2-associated modulatory protein gene) in male mice causes sperm malformation and infertility. *J Biol Chem* 288: 15167 – 15180

Lee JY, Stearns T (2013) FOP is a centriolar satellite protein involved in ciliogenesis. *PLoS ONE* 8: e58589

Lee SH, Lee MS, Choi TI, Hong H, Seo JY, Kim CH, Kim J (2016) MCRS1 associates with cytoplasmic dynein and mediates pericentrosomal material recruitment. *Sci Rep* 6: 27284

Liu J, Li J, Li P, Wang Y, Liang Z, Jiang Y, Li J, Feng C, Wang R, Chen H *et al* (2017) Loss of DLG5 promotes breast cancer malignancy by inhibiting the Hippo signaling pathway. *Sci Rep* 7: 42125

Liu Y, Gupta GD, Barnabas DD, Agircan FG, Mehmood S, Wu D, Coyaud E, Johnson CM, McLaughlin SH, Andreeva A *et al* (2018) Direct binding of CEP85 to STIL ensures robust PLK4 activation and efficient centriole assembly. *Nat Commun* 9: 1731

Lopes CA, Prosser SL, Romio L, Hirst RA, O'Callaghan C, Woolf AS, Fry AM (2011) Centriolar satellites are assembly points for proteins implicated in human ciliopathies, including oral-facial-digital syndrome 1. *J Cell Sci* 124: 600 – 612

Lucker BF, Behal RH, Qin H, Siron LC, Taggart WD, Rosenbaum JL, Cole DG (2005) Characterization of the intraflagellar transport complex B core: direct interaction of the IFT81 and IFT74/72 subunits. *J Biol Chem* 280: 27688 – 27696

Luders J, Stearns T (2007) Microtubule-organizing centres: a re-evaluation. *Nat Rev* 8: 161 – 167

Maia AR, Zhu X, Miller P, Gu G, Maiato H, Kaverina I (2013) Modulation of Golgi-associated microtubule nucleation throughout the cell cycle. *Cytoskeleton (Hoboken)* 70: 32 – 43

Martin ME, Berk AJ (1998) Adenovirus E1B 55K represses p53 activation in vitro. *J Virol* 72: 3146 – 3154

Martinez-Garay I, Rustom A, Gerdes HH, Kutsche K (2006) The novel centrosomal associated protein CEP55 is present in the spindle midzone and the midbody. *Genomics* 87: 243 – 253

McGough IJ, Steinberg F, Gallon M, Yatsu A, Ohbayashi N, Heesom KJ, Fukuda M, Cullen PJ (2014) Identification of molecular heterogeneity in SNX27-retromer-mediated endosome-to-plasma-membrane recycling. *J Cell Sci* 127: 4940 – 4953

Meitinger F, Anzola JV, Kaulich M, Richardson A, Stender JD, Benner C, Glass CK, Dowdy SF, Desai A, Shiau AK *et al* (2016) 53BP1 and USP28 mediate p53 activation and G1 arrest after centrosome loss or extended mitotic duration. *J Cell Biol* 214: 155 – 166

Mojarad BA, Gupta GD, Hasegan M, Goudiam O, Basto R, Gingras AC, Pelletier L (2017) CEP19 cooperates with FOP and CEP350 to drive early steps in the ciliogenesis programme. *Open Biol* 7: 170114

Moser JJ, Fritzler MJ, Rattner JB (2011) Repression of GW/P body components and the RNAi microprocessor impacts primary ciliogenesis in human astrocytes. *BMC Cell Biol* 12: 37

Nachury MV, Loktev AV, Zhang Q, Westlake CJ, Peranen J, Merdes A, Slusarski DC, Scheller RH, Bazan JF, Sheffield VC *et al* (2007) A core complex of BBS proteins cooperates with the GTPase Rab8 to promote ciliary membrane biogenesis. *Cell* 129: 1201 – 1213

Obino D, Farina F, Malbec O, Saez PJ, Maurin M, Gaillard J, Dingli F, Loew D, Gautreau A, Yuseff MI *et al* (2016) Actin nucleation at the centrosome controls lymphocyte polarity. *Nat Commun* 7: 10969

Odabasi E, Gul S, Kavakli L, Firat-Karalar EN (2019) Centriolar satellites are required for efficient ciliogenesis and ciliary content regulation. *EMBO Rep* 20: e47723

Patzke S, Hauge H, Sioud M, Finne EF, Sivertsen EA, Delabie J, Stokke T, Aasheim HC (2005) Identification of a novel centrosome/microtubule-associated coiled-coil protein involved in cell-cycle progression and spindle organization. *Oncogene* 24: 1159 – 1173

Petry S, Vale RD (2015) Microtubule nucleation at the centrosome and beyond. *Nat Cell Biol* 17: 1089 – 1093

Rai AK, Chen JX, Selbach M, Pelkmans L (2018) Kinase-controlled phase transition of membraneless organelles in mitosis. *Nature* 559: 211 – 216

Regnard C, Fesquet D, Janke C, Boucher D, Desbruyeres E, Koulakoff A, Insina C, Travo P, Edde B (2003) Characterisation of PGs1, a subunit of a protein complex co-purifying with tubulin polyglutamylase. *J Cell Sci* 116: 4181 – 4190

Roux KJ, Kim DI, Raida M, Burke B (2012) A promiscuous biotin ligase fusion protein identifies proximal and interacting proteins in mammalian cells. *J Cell Biol* 196: 801 – 810

Sanjana NE, Shalem O, Zhang F (2014) Improved vectors and genome-wide libraries for CRISPR screening. *Nat Methods* 11: 783 – 784

Sergouniotis PI, Chakarova C, Murphy C, Becker M, Lenassi E, Arno G, Lek M, MacArthur DG, Consortium UC-E, Bhattacharya SS *et al* (2014) Biallelic variants in TTLL5, encoding a tubulin glutamylase, cause retinal dystrophy. *Am J Hum Genet* 94: 760 – 769

Silva E, Betleja E, John E, Spear P, Moresco JJ, Zhang S, Yates JR III, Mitchell BJ, Mahjoub MR (2016) Ccdc11 is a novel centriolar satellite protein essential for ciliogenesis and establishment of left-right asymmetry. *Mol Biol Cell* 27: 48 – 63

Spektor A, Tsang WY, Khoo D, Dynlacht BD (2007) Cep97 and CP110 suppress a cilia assembly program. *Cell* 130: 678 – 690

Staples CJ, Myers KN, Beveridge RD, Patil AA, Howard AE, Barone G, Lee AJ, Swanton C, Howell M, Maslen S *et al* (2014) Ccdc13 is a novel human centriolar satellite protein required for ciliogenesis and genome stability. *J Cell Sci* 127: 2910 – 2919

Staples CJ, Myers KN, Beveridge RD, Patil AA, Lee AJ, Swanton C, Howell M, Boulton SJ, Collis SJ (2012) The centriolar satellite protein Cep131 is important for genome stability. *J Cell Sci* 125: 4770 – 4779

Stegmeier F, Sowa ME, Nalepa G, Gygi SP, Harper JW, Elledge SJ (2007) The tumor suppressor CYLD regulates entry into mitosis. *Proc Natl Acad Sci USA* 104: 8869 – 8874

Stowe TR, Wilkinson CJ, Iqbal A, Stearns T (2012) The centriolar satellite proteins Cep72 and Cep290 interact and are required for recruitment of BBS proteins to the cilium. *Mol Biol Cell* 23: 3322 – 3335

Tanaka N, Meng W, Nagae S, Takeichi M (2012) Nezha/CAMSAP3 and CAMSAP2 cooperate in epithelial-specific organization of noncentrosomal microtubules. *Proc Natl Acad Sci USA* 109: 20029 – 20034

Tang Z, Lin MG, Stowe TR, Chen S, Zhu M, Stearns T, Franco B, Zhong Q (2013) Autophagy promotes primary ciliogenesis by removing OFD1 from centriolar satellites. *Nature* 502: 254 – 257

Teo G, Liu G, Zhang J, Nesvizhskii AI, Gingras AC, Choi H (2014) SAINTexpress: improvements and additional features in Significance Analysis of INTeractome software. *J Proteomics* 100: 37 – 43

Thein KH, Kleylein-Sohn J, Nigg EA, Gruneberg U (2007) Astrin is required for the maintenance of sister chromatid cohesion and centrosome integrity. *J Cell Biol* 178: 345 – 354

Villumsen BH, Danielsen JR, Povlsen L, Sylvestersen KB, Merdes A, Beli P, Yang YG, Choudhary C, Nielsen ML, Mailand N *et al* (2013) A new cellular stress response that triggers centriolar satellite reorganization and ciliogenesis. *EMBO J* 32: 3029 – 3040

Wang L, Lee K, Malonis R, Sanchez I, Dynlacht BD (2016) Tethering of an E3 ligase by PCM1 regulates the abundance of centrosomal KIAA0586/Talpid3 and promotes ciliogenesis. *Elife* 5: e12950

Wippich F, Bodenmiller B, Trajkovska MG, Wanka S, Aebersold R, Pelkmans L (2013) Dual specificity kinase DYRK3 couples stress granule condensation/dissolution to mTORC1 signaling. *Cell* 152: 791 – 805

Wong YL, Anzola JV, Davis RL, Yoon M, Motamedi A, Kroll A, Seo CP, Hsia JE, Kim SK, Mitchell JW *et al* (2015) Cell biology. Reversible centriole depletion with an inhibitor of Polo-like kinase 4. *Science* 348: 1155 – 1160

Yeh C, Coyaud E, Bashkurov M, van der Lelij P, Cheung SW, Peters JM, Raught B, Pelletier L (2015) The deubiquitinase USP37 regulates chromosome cohesion and mitotic progression. *Curr Biol* 25: 2290 – 2299

Youn JY, Dunham WH, Hong SJ, Knight JDR, Bashkurov M, Chen GI, Bagci H, Rathod B, MacLeod G, Eng SWM *et al* (2018) High-density

proximity mapping reveals the subcellular organization of mRNA-associated granules and bodies. *Mol Cell* 69: 517 – 532.e11

Zhang W, Kim PJ, Chen Z, Lokman H, Qiu L, Zhang K, Rozen SG, Tan EK, Je HS, Zeng L (2016) MiRNA-128 regulates the proliferation and neurogenesis of neural precursors by targeting PCM1 in the developing cortex. *Elife* 5: e11324

Zhao WM, Seki A, Fang G (2006) Cep55, a microtubule-bundling protein, associates with centralspindlin to control the midbody integrity and cell abscission during cytokinesis. *Mol Biol Cell* 17: 3881 – 3896

Zimmermann M, Murina O, Reijns MAM, Agathanggelou A, Challis R, Tarnauskaite Z, Muir M, Fluteau A, Aregger M, McEwan A *et al* (2018) CRISPR screens identify genomic ribonucleotides as a source of PARP-trapping lesions. *Nature* 559: 285 – 289